Geochemistry, Geophysics, Geosystems®

AGU ADVANCING EARTH AND SPACE SCIENCES

RESEARCH ARTICLE
10.1029/2023GC011072

Exhumed Serpentinites and Their Tectonic Significance in Non-Collisional Orogens

Damián Donoso-Tapia[1], Kennet E. Flores[1], Celine Martin[2], Esteban Gazel[3], and Jeffrey Marsh[4]

[1]Department of Earth, Marine and Environmental Sciences, University of North Carolina, Chapel Hill, NC, USA, [2]Department of Earth and Planetary Sciences, American Museum of Natural History, New York, NY, USA, [3]Department of Earth and Atmospheric Sciences, Cornell University, Ithaca, NY, USA, [4]Mineral Exploration Research Centre, Harquail School of Earth Sciences, Laurentian University, Sudbury, ON, Canada

Key Points:

- Serpentinites associated with HP–LT rocks are common in the Andes, but their origin and tectonic significance are not fully understood
- Our results in Cordillera Real serpentinites suggest four sources derived from the mantle wedge and obducted ophiolites
- Serpentinites in non-collisional orogens are exhumed during slab rollback and back-arc basin closure phases

Supporting Information:

Supporting Information may be found in the online version of this article.

Correspondence to:

K. E. Flores,
keflores@unc.edu

Citation:

Donoso-Tapia, D., Flores, K. E., Martin, C., Gazel, E., & Marsh, J. (2024). Exhumed serpentinites and their tectonic significance in non-collisional orogens. *Geochemistry, Geophysics, Geosystems*, *25*, e2023GC011072. https://doi.org/10.1029/2023GC011072

Received 24 AUG 2023
Accepted 9 FEB 2024

Author Contributions:

Conceptualization: Kennet E. Flores
Data curation: Damián Donoso-Tapia, Celine Martin, Esteban Gazel
Formal analysis: Damián Donoso-Tapia
Funding acquisition: Kennet E. Flores, Celine Martin, Jeffrey Marsh
Investigation: Damián Donoso-Tapia, Kennet E. Flores, Jeffrey Marsh
Methodology: Damián Donoso-Tapia, Kennet E. Flores, Celine Martin, Esteban Gazel
Project administration: Kennet E. Flores, Celine Martin
Resources: Damián Donoso-Tapia, Kennet E. Flores, Esteban Gazel

Abstract Exhumed serpentinites are fragments of ancient oceanic lithosphere or mantle wedge that record deep fluid-rock interactions and metasomatic processes. While common in suture zones after closure of ocean basins, in non-collisional orogens their origin and tectonic significance are not fully understood. We study serpentinite samples from five river basins in a segment of the non-collisional Andean orogen in Ecuador (Cordillera Real). All samples are fully serpentinized with antigorite as the main polymorph, while spinel is the only relic phase. Watershed delineation analysis and in-situ B isotope data suggest four serpentinite sources, linked to mantle wedge ($\delta^{11}B = \sim -10.6$ to -0.03‰) and obducted ophiolite ($\delta^{11}B = -2.51$ to $+5.73$‰) bodies, likely associated with Triassic, Jurassic-Early Cretaceous, and potentially Late Cretaceous-Paleocene high-pressure (HP)–low-temperature metamorphic sequences. Whole-rock trace element data and in-situ B isotopes favor serpentinization by a crust-derived metamorphic fluid. Thermodynamic modeling in two samples suggests serpentinization at ~550–500°C and pressures from 2.5 to 2.2 GPa and 1.0–0.6 GPa for two localities. Both samples record a subsequent overprint at ~1.5–0.5 GPa and 680–660°C. In the Andes, regional phases of slab rollback have been reported since the mid-Paleozoic to Late Cretaceous. This tectonic scenario favors the extrusion of HP rocks into the forearc and the opening of back-arc basins. Subsequent compressional phases trigger short-lived subduction in the back-arc that culminates with ophiolite obduction and associated metamorphic rock exhumation. Thus, we propose that serpentinites in non-collisional orogens are sourced from extruded slivers of mantle wedge in the forearc or obducted ophiolite sequences associated with regional back-arc basins.

Plain Language Summary Serpentinites are metamorphic rock products of fluid-mediated alteration of the mantle. They occur in the ocean floor and the core of mountain belts resulting from continental collisions after the closure of ancient oceanic basins. However, their origin in non-collisional mountain belts, such as the Andes, remains unclear. To address this conundrum, we studied serpentinite boulders from five river basins in the Ecuadorian northern Cordillera Real. We found that rocks are composed of the high-temperature serpentine mineral, while spinel is the only original mineral preserved. River basin analysis and boron stable isotopes indicate four potential sources for the studied rocks, juxtaposed to rocks ranging in age from ~240 to 55 million. Bulk-rock chemistry and boron isotopes suggest that the serpentinization was triggered by crustal fluids at depths between 80 and 30 km in a subduction zone environment. Through time, the Andes have been characterized by extensional and compressional tectonic phases. These tectonic scenarios enhance the extraction of rocks at deep sections of the Earth along major faults. We propose that Andean serpentinites are fragments of the Earth's mantle sourced from ancient subduction zones and back-arc basins.

1. Introduction

Serpentinites are the product of the hydration of ultramafic rocks, where the primary mineral assemblage is partially or fully replaced by serpentine polymorphs (antigorite, lizardite, and chrysotile). In subduction zone settings, the serpentinization process can occur by infiltration of seawater into the oceanic lithosphere at the outer rise bend or by release of volatiles from subducted slabs through dehydration reactions that hydrothermally alter the overlying mantle wedge (e.g., K. A. Evans et al., 2013; Guillot et al., 2009). The high volatile content of serpentinites (up to 15 w.t%) makes them critical rocks for understanding transport and recycling of elements, their role in the genesis of arc magmas, transport of volatiles to the Deep Earth, and nature of fluids responsible for

Supervision: Kennet E. Flores
Validation: Esteban Gazel
Visualization: Kennet E. Flores, Celine Martin, Jeffrey Marsh
Writing – original draft: Damián Donoso-Tapia
Writing – review & editing: Damián Donoso-Tapia, Kennet E. Flores, Celine Martin, Esteban Gazel, Jeffrey Marsh

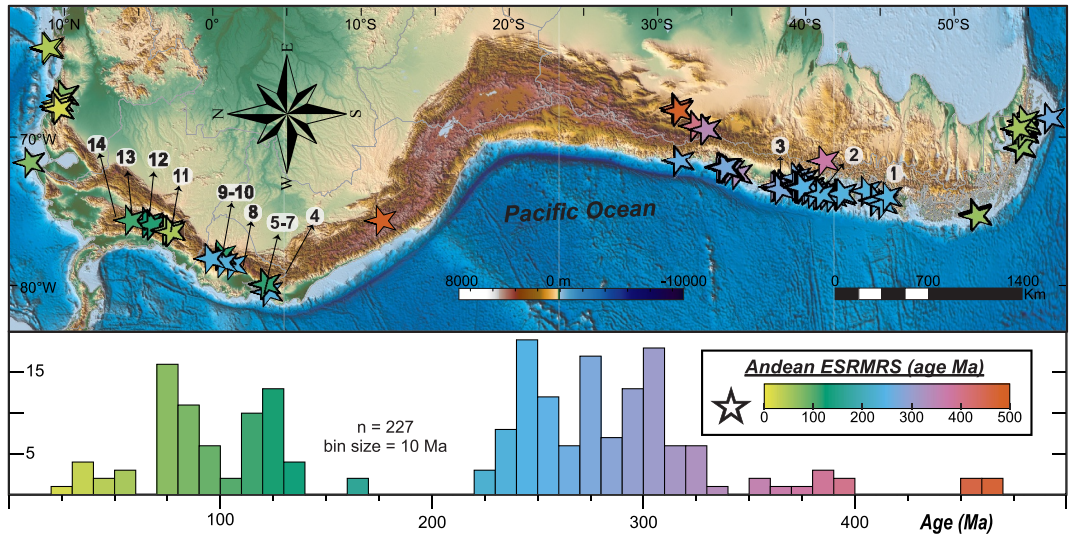

Figure 1. Geographical and age distribution of Andean of exhumed subduction-related metamorphic rocks (ESRMRS) and serpentinite occurrences. Circled numbers indicate serpentinite-bearing complexes: 1. Eastern Andean Metamorphic Complex; 2. Cuesta Brava; 3. La Cabaña; 4. Zumba; 5. Quebrada Seca; 6. El Toro; 7. Palenque; 8. Guarguallá; 9. Quebrada Soledad; 10. El Carmen; 11. Jambalo; 12. Barragan; 13. Pijao; 14. Medellín (references in the main text). ESRMRS from Angiboust et al. (2017, 2018), Avellaneda-Jiménez et al. (2022), Bocchio et al. (1996), Brook (1984), A. Bustamante (2008), A. Bustamante et al. (2011, 2012), Casquet et al. (2001), Davis et al. (1999), Duhart and Adriasola (2008), Duhart et al. (2001), Feininger and Silberman (1982), Flores et al. (2019), Gabriele (2002), García-Ramírez et al. (2017), Glodny et al. (2005, 2008), González-Jiménez et al. (2017), Grunow et al. (1992), Halpern (1973), Hervé et al. (1981), Höfer et al. (2001), Hyppolito et al. (2014, 2016), John et al. (2010), Kato and Godoy (1995), Kato et al. (2008), Kohn et al. (1995), Maloney et al. (2011), Martínez et al. (2012), Ramos et al. (1998), Romero et al. (2018), Sisson et al. (1997, 2005), Smith et al. (1999), Stöckhert et al. (1995), Toussaint and Restrepo (1978), van Staal et al. (2011), Viete et al. (2015), Vujovich et al. (2004), Weber et al. (2007, 2011), Willner (2005), Willner et al. (2004, 2005, 2009, 2011, 2012, 2014), and references therein.

serpentinization (e.g., Alt et al., 2012; Deschamps et al., 2013; Martin et al., 2020; Pagé et al., 2018; Peters et al., 2017).

Accreted and exhumed serpentinites commonly occur along modern convergent boundaries and suture zones. They mark plate boundaries resulting from accretion of oceanic crust or obduction and exhumation during ocean basin shortening and closure, leading to continental collisions (e.g., Agard et al., 2014; B. W. Evans et al., 2013; Guillot et al., 2009). However, they may also indicate inversion and closure of mafic-floored back-arc basins (Hässig et al., 2016; Rojo et al., 2021). Serpentinites within suture zone complexes are often associated with exhumed subduction-related metamorphic rocks (ESRMRS, e.g., blueschist, eclogite) complexes. Their origin is linked either to slivers of hydrated mantle from the subducted slab or sections of the subduction interface and mantle wedge (e.g., Flores et al., 2013; John et al., 2010; Martin et al., 2020; Schwartz et al., 2000). Discrete serpentinite bodies have also been reported in association with ESRMRS complexes in non-collisional settings (e.g., the Andes; Figure 1). Their low density makes them inherently buoyant in the subduction interface, thus facilitating their ascent during material offscraping and incorporation into the accretionary prism along with lithologies of higher density, such as blueschist- or eclogite-facies rocks (e.g., Agard et al., 2009; Sanhueza et al., 2022; Tamblyn et al., 2019).

Orogens are the product of penetrative crustal deformation and magmatism in convergent margins that produce crustal thickening. They are commonly classified as cordilleran/accretionary/non-collisional or collisional. While non-collisional orogens are ubiquitous in oceanic realms around continents, collisional orogens generally represent the last shortening phase during continental amalgamation (e.g., Cawood et al., 2009; Dewey & Bird, 1970). The Andes is one of the most intriguing and well-studied non-collisional orogens on Earth, and there is evidence of a Precambrian-Paleozoic collisional stage during the amalgamation of Gondwana (e.g., Ramos, 1988, 2008). No major collisional events have been reported after the late Devonian. In this contribution, paleo-Andes orogeny refers to the non-collisional stage starting at c. 360 Ma until the onset of the last compressional phase (modern Andean orogeny) at c. 50 Ma (Faccenna et al., 2017).

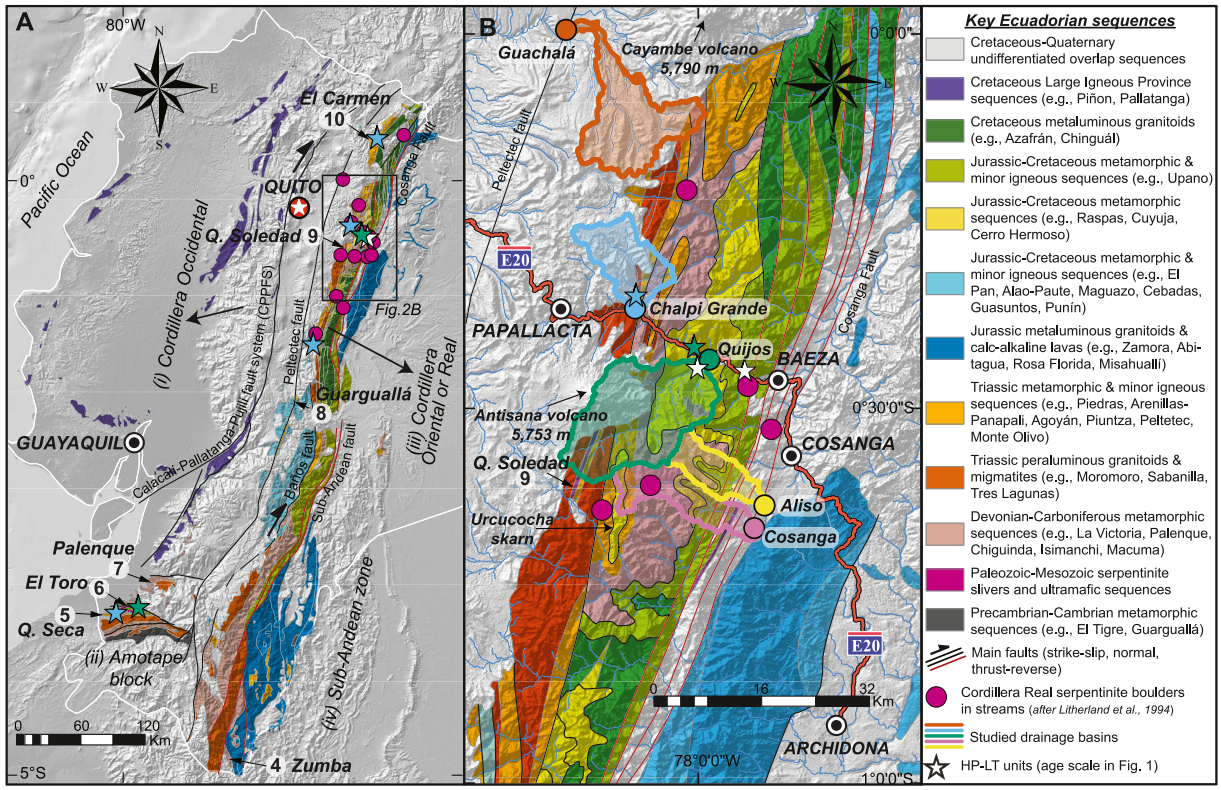

Figure 2. Geology of the study area in the Ecuadorian Andes. (a) Tectonostratographic domains and key geologic features of Ecuador (after Aspden et al., 1995; Eguez et al., 2017; Litherland et al., 1994). (b) Study region showing the location of the collected samples and their potential source associated to the drainage area of the rivers after watershed delineation analysis.

Tracing the origin of serpentinites in subduction settings is a major challenge, as their inherent heterogeneity, serpentinization fluid source, and the extent of element mobilization make it difficult to discriminate between an abyssal or a mantle wedge genesis. Studies have attempted to address the petrogenesis of serpentinites by using whole-rock major and trace elements, and even though certain trends in data exist, the overlap regions are generally large (e.g., Niu, 2004; Peters et al., 2017). Approaches through whole-rock stable isotopes (e.g., δD, $\delta^{11}B$, $\delta^{13}C$, $\delta^{18}O$, $\delta^{34}S$) appear to be a reliable tool to characterize the fluid responsible for serpentinization and the tectonic setting where it took place (Alt et al., 2012; Prigent et al., 2018; Raia et al., 2022). However, in serpentinites with multiple serpentinization events, a whole-rock approach may not be suitable to discern potential differences in their isotopic signatures. In contrast, in-situ boron isotope studies ($\delta^{11}B$) allow to characterize each serpentine generation, providing insight into their origin and potential fluid mixing (Martin et al., 2015, 2016, 2020, 2023). Boron, a highly fluid-mobile element (FME), with its two isotopes (^{10}B and ^{11}B) that have a large relative mass difference, is predicted to fractionate easily as a function of temperature, pH, phase partitioning, and potentially depth (Martin et al., 2020; Wunder et al., 2005). ^{10}B is preferentially partitioned in tetrahedral sites of solid phases, usually phyllosilicates, whereas ^{11}B does so in trigonal sites of fluid phases (Marschall et al., 2007; Wunder et al., 2005).

In this study, we present mineral chemistry, whole-rock, and in-situ boron isotope data of 13 serpentinites collected in the stream network of the northern Cordillera Real, Ecuador (Figure 2). The main goal is to assess their source, petrogenesis, metamorphism, and characterize the fluids responsible for serpentinization. We will integrate our findings with compiled data of ESRMRS of different ages along the Andean orogen to unravel the role of serpentinites in non-collisional orogens.

2. Geological Setting and Sample Description

The Andes encloses widespread occurrences of Early Ordovician to Oligocene ESRMRS (Figure 1) linked to the amalgamation of western Gondwana, the paleo-Andean orogeny, and Cretaceous back-arc closures and the

collision of an oceanic Large Igneous Province (LIP) (Donoso-Tapia et al., 2022). At least 14 serpentinite and ultramafic complexes have been described in association with paleo-Andean ESRMRS and ophiolitic sequences. These units are commonly scarce and occur in difficult access areas in southern Chile and the northern Andes in Ecuador and Colombia. Thus, the limited studies focused on these rocks have linked them to exhumation of slab sections (González-Jiménez et al., 2017; John et al., 2010) or obduction of back-arc basins (Garcia-Casco et al., 2020; Rojo et al., 2021). These proposed tectonic scenarios are uncommon in non-collisional orogens and more related to collisional events during shortening and continent amalgamation.

The modern Ecuadorian Andes are divided into fault-bounded tectonostratigraphic domains (Figure 2a). From west to east, the (a) Cordillera Occidental, which consists of LIP sequences that collided with the South American margin at ~75–55 Ma (George et al., 2021; Spikings et al., 2015; Villagómez et al., 2011); (b) The coastal Amotape Block and (c) the Cordillera Oriental or Real consists of Cambrian-Precambrian metamorphic basement, Devonian to Cretaceous sedimentary and igneous sequences that underwent various metamorphic events, and Triassic to Cretaceous peraluminous and metaluminous granitoids and migmatites (e.g., Aspden & Litherland, 1992; Aspden et al., 1995; Litherland et al., 1994; Spikings et al., 2015, 2021); finally, (d) the sub-Andean zone is characterized by deformed thrust belts, including Precambrian migmatitic gneiss, Triassic-Jurassic sedimentary and volcanic sequences, and Jurassic metaluminous granitoids (e.g., Chiaradia et al., 2008; Litherland et al., 1994; Romeuf et al., 1995; Spikings et al., 2001).

Based on widespread relics of high-pressure–low-temperature (HP–LT) rocks in the basement of the Ecuadorian Cordillera Real (Figure 2), an Early Cretaceous collision between South America and a continental fragment was proposed by Massonne and Toulkeridis (2012). Our ongoing research on this region confirms the presence of widespread HP–LT rocks, but with peak ages of Late Triassic, Early Cretaceous, and Late Cretaceous-Paleocene (Flores et al., 2019). Similar metamorphic ages in ESRMRS have been reported in the Ecuadorian Amotape block and Colombia (A. Bustamante et al., 2011, 2012; Gabriele, 2002; García-Ramírez et al., 2017; John et al., 2010), indicating a regional distribution in the northern Andes.

Serpentinites and other ultramafic rocks outcrop in the Amotape block and the Cordillera Real domains (Figure 2a). In the first one, they occur as W-E-oriented slivers tectonically associated with units of El Oro Metamorphic Complex; the Devonian Palenque mélange, the Triassic Piedras unit, and the Early Cretaceous Raspas Complex, respectively (Aspden et al., 1995; Gabriele, 2002; Litherland et al., 1994; Suhr et al., 2019). Ultramafic units in Palenque mainly comprise serpentinite bodies associated with minor gabbros and gabbroic pegmatites. The Triassic Piedras unit consists mainly of coarse- to fine-grained amphibolites with local lenses of serpentinites exposed near the village of Quebrada Seca and along the southern section of the Tahuín Dam Lake. The eclogite-facies ultramafics of the Raspas Complex are grouped as the El Toro Formation and consist of massive metaperidotite with mafic bands and minor serpentinite crosscut by mafic eclogitic dikes. Geochemical and isotopic studies suggest that El Toro metaperidotites and the HP–LT mafic and metasedimentary rocks of Raspas Complex represent an exhumed section of a coherent slab (Halama et al., 2013; Herms et al., 2012; John et al., 2010).

The Cordillera Real ultramafic counterparts occur as N-S-oriented tectonic slivers within the metamorphic sequences (Figure 2a). The southernmost sliver occurs near the locality of Zumba, where serpentinites are associated with pyroxenites and gabbros, likely of Triassic age (Litherland et al., 1994). In the central Cordillera Real, a serpentinite sliver is sandwiched between Precambrian-Cambrian metagabbros and Triassic metabasalt and metasedimentary sequences defined as the Guarguallá unit and the Peltetec ophiolitic belt, respectively (Spikings et al., 2021; Villares et al., 2021). Further north, two serpentinite slivers were described by Litherland et al. (1994), one at ~4,000 m.a.s.l. in the Quebrada Soledad on the south slope of the Antisana Volcano and the second near the El Carmen River. Both slivers are tectonically juxtaposed to pelitic schists and paragneisses of the Paleozoic-Triassic Agoyán unit (Cochrane et al., 2014a). The El Carmen body is a sheared fuchsitic serpentinite exposed near the Triassic Monte Olivo amphibolite. Serpentinites from Quebrada Soledad consist of a 30 m west-dipping belt bounded by gray and black phyllite sequences. Litherland et al. (1994) reported serpentinite boulders in at least 10 river basins within the northern Cordillera Real between the Antisana and Cayambe volcanoes (Figure 2b). Based on the abundance and large size of serpentinite boulders in streams, Litherland et al. (1994) proposed the potential occurrence of serpentinites around the Urcucocha skarn field (blocks in the western Chiriyacu Creek and eastern upper Cosanga River) and the lower Cosanga River (blocks of 6 × 5 m in size). The latter potentially occurs tectonically associated with the metamafic and metapelite sequence of the Late Cretaceous Upano unit.

The 13 serpentinite boulders were sampled from five river basins above 2,140 m.a.s.l. and along a ∼50 km transect in the northern Cordillera Real (Figure 2b). The boulders have overall low sphericity. However, their size and roundness vary from river to river (Figure S1 in Supporting Information S1). From west to east, the Guachalá River samples (3 samples; 0°00′19.71″ N–78°10′30.64″ W. Figure S1A in Supporting Information S1) are subangular and up to 140 × 80 cm in size and were found along volcanic blocks. In the Chalpi Grande River (4 samples; 0°21′59.91″ S–78°05′06.22″ W. Figures S1B and S1C in Supporting Information S1), the sampled serpentinites are angular and up to 30 × 20 cm in size and were found along blocks of garnet schists, metaigneous, and metasedimentary rocks from the Devonian-Carboniferous Chiguinda, and Triassic Tres Lagunas and Agoyán units. The Quijos river serpentinites (3 samples; 0°26′13.71″ S–77° 59′06.72″ W. Figures S1D–S1F in Supporting Information S1) vary in sizes from metric (3 × 2 m) to centimetric (40 × 20 cm). At this locality, serpentinite boulders occur alongside blocks of Chiguinda and Agoyán units but also include marbles and garnet schist boulders from the Jurassic Cerro Hermoso and Cuyuja units. Additionally, centimetric (50 × 30 cm) blocks of sodic-calcic amphibole and mica-bearing mafic schists of an unknown unit were also sampled. Serpentinites from the Aliso River (1 sample; 0°37′44.77″ S–77°54′38.65″ W. Figure S1G in Supporting Information S1) are subrounded and 40 × 20 cm in size; they were found alongside blocks of mafic rocks of the Upano unit, and limestone and sandstone from Cretaceous overlap sequences. The Cosanga River samples (2 samples; 0°39′42.80″ S–77°55′22.14″ W. Figures S1H–S1I in Supporting Information S1) are subangular metric (3 × 2 m) and centimetric (70 × 50 cm) boulders, associated with similar blocks found in the Aliso river locality.

3. Analytical Methods

Watershed delineation for each sampled river (Figure 2b) was carried out using R software, based on the sampling location and digital elevation data built from the USGS EarthExplorer Shuttle Radar Topography Misssion images at 3-arc-seconds resolution of the study area. The delineated areas were overlaid on the geological map (after Litherland et al., 1994) to constrain the boulders provenance, and drainage area estimates (km^2) were calculated using Quantum Geographic Information System software (QGIS). The thin sections of the studied sample were petrographically and texturally characterized using a polarized light microscope (PLM) and a Vega TS 5136 Tescan scanning electron microscope at the University of North Carolina at Chapel Hill. Operating conditions were under high vacuum, 15 kV, and 1–5 nA. Back-scattered electron imaging and X-ray energy-dispersive spectrometry analysis were carried out in representative mineral phases of all thin sections.

Serpentine polymorphs were differentiated using a WITec Alpha 300R Confocal Raman microscope at Cornell University. Raman signal was acquired over 30 s in three accumulating cycles, with laser output power between 3 and 10 mW, and using 300 and 1,800 lines/mm grating. Spectra identification and processing were done using FIVE software from WITec and the ChemoSpec (Hanson, 2014) package for R software.

Mineral phase compositions were obtained using a Cameca SX5-Tactis electron-probe microanalyzer (EMPA) at the American Museum of Natural History. Mineral analytical conditions were 15 kV accelerating voltage, 20 nA beam current, and 1–2 μm electron beam diameter. Counting rates were 30 s on peaks and 15 s on backgrounds. Analytical standards were well-characterized natural and synthetic minerals, including Wakefield diopside (Si, Mg, Ca), rutile (Ti), albite (Al, Na), magnesiochromite (Cr), fayalite (Fe), rhodonite (Mn), orthoclase (K), CoS (Co), NiS (Ni), and ZnS (Zn). All element detection limits are ∼0.01 wt%, and all reported values are above. We did not apply any post-processing correction for the effect of inferred H_2O content. Mineral abbreviations are after Whitney and Evans (2010). Stoichiometry calculations were based on the MinPlot software database (Walters, 2022 and references therein). In the case of antigorite, stoichiometry was determined based on 116 oxygens, corresponding to the antigorite polysome in well-crystallized serpentinites (see Mellini et al., 1987; Padrón-Navarta et al., 2011).

Whole-rock major and trace elements were determined at the Hamilton Analytical Laboratory. Loss of ignition (LOI) values were measured by overnight heating the samples in silica crucibles at 900°C. X-ray fluorescence (XRF) analyzed major elements using a Thermo ARL Perform'X spectrometer. Trace elements were estimated by laser ablation inductively coupled-plasma mass spectrometry (LA-ICP-MS) using an Applied Spectra RESOlution-SE laser ablation system equipped with an ArF Excimer 193 nm laser coupled to an Agilent 8900 QQQ ICP-MS. Operating conditions were 5 Hz repetition rate, 10 ms dwell time, and 5 J/cm^2 fluence. The spot

diameter was 100 μm; the analyzed standards were BHVO-1 and PCC-1. Data were processed using the Iolite software (Paton et al., 2011). Trace element data presented in the text and figures correspond to LA-ICP-MS data, whereas major element data is only XRF.

Geothermobarometric estimations for two suitable serpentinite samples (Chalpi Grande E16-7-3; Cosanga E16-1-7) were calculated by thermodynamic modeling using the Perple_X software (Connolly, 2005). Pseudosections were generated in the CFMASH system using whole-rock XRF data combined with antigorite and tremolite mineral isopleths under water-saturated conditions. We used version 6.9.1 with the thermodynamic database of Holland and Powell (2011), version DS622. Solution models included in the pseudosection are as follows: antigorite—Atg (Padrón-Navarta et al., 2013), olivine—O, garnet—Gt and chlorite—Chl (Holland & Powell, 1998), orthopyroxene—Opx (Powell & Holland, 1999), clinopyroxene (Jennings & Holland, 2015), talc—T (ideal), and clinoamphibole—cAmph (Green et al., 2016). Antigorite and tremolite isopleths were generated following the same solution models mentioned above. To further constrain the pressure and temperature (P-T) conditions attained by the serpentinites, we used aluminum in antigorite (Al-in-Atg) and tremolite X_{Mg} (Mg/(Mg + Fe)) isopleths, which are reliable thermobarometers in the absence of serpentine dehydration products or other typical silicate phases used in thermodynamic modeling, such as garnet (Butjosa et al., 2023; Padrón-Navarta et al., 2013; Shen et al., 2015).

In-situ boron isotopes and critical trace elements (Li, B, Cr, Ni, As, Sr, Y, Sb, Cs, Pb, U) concentration were measured on epoxy resin mounts in two separate sessions, targeting mineral phases including antigorite, chlorite, and amphibole. Boron isotopes were estimated by laser ablation multi-collector inductively coupled-plasma mass spectrometry (LA-MC-ICP-MS), using an ESI New Wave UP-193-FX ArF*(nm) excimer laser coupled to a Neptune Plus (ThermoScientific) at the Lamont Doherty Earth Observatory following the method developed by Martin et al. (2015). The instrument was set up with Ni/Jet X cones and an RF power of 1,100 W. The data were collected by electron multipliers with a repetition rate of 10 Hz and a fluence of ∼10 J/cm^2 at a speed of 3 μm per second, along traverses of ∼250–300 μm length with spot diameters between 25 and 125 μm. The standard NIST SRM 612 was used to monitor the boron isotope measurements, yielding $\delta^{11}B$ of +0.77 ± 1.71‰ (2 S.D., $n = 81$). The synthetic glass SRM 610 was run as an unknown, yielding $\delta^{11}B$ values of −0.31 ± 5.23‰ (2 S.D., $n = 5$).

In-situ key trace elements on the same mineral phases were performed at the Cornell University LA-ICP-MS (CMaS) facility using an Agilent 8900 equipped with an ESI NWR 193HE laser. All analyses were done in similar operating conditions of 10 Hz repetition rate; dwell time was 10 ms (Cr, Ni, Sr, Y, Cs, Pb, U) and 20 ms (Li, B, As, Sb), ablation time was set to 30 s, and 10 J/cm^2 fluence. Spot sizes range from 50 to 100 μm depending on mineral size. The five external standards used are AGV-2, BCR-2, BHVO-2, BIR-1, and NIST SRM 612. Data processing was done using Iolite software.

4. Results

4.1. Watershed Delineation Analysis

The studied samples were collected in five streams that define varying hydrographic basins from the collecting sites (Figure 2b). The Guachalá River basin (178 km^2) is the only one that drains toward the western flank of the Cordillera Real. The Chalpi Grande and Quijos rivers erode the core section of the Cordillera Real in the study area. The Chalpi Grande River is a tributary of the Papallacta River and, from the sampling site, defines a basin of 101 km^2. The Quijos River has the largest hydrographic basin of 269 km^2, and it is the only one that potentially receives sediment input from the Quebrada Soledad serpentinite outcrop. The Aliso and Consanga rivers drain the eastern flank of the Cordillera Real and define basin areas of 68 and 106 km^2, respectively.

The Guachalá and Chalpi Grande delineated basins predict sediment sources from Devonian-Carboniferous and Triassic metamorphic and igneous sequences (Chiguinda, Tres Lagunas, Agoyán) and potential sources covered by the modern volcanic sequences. The Quijos hydrographic basin contains the abovementioned lithologies and the Jurassic-Cretaceous metamorphic sequences from Cuyuja and Cerro Hermoso units. Aliso basin is limited to lithologies of Chiguinda and the Jurassic-Cretaceous metamorphic and minor igneous sequences of the Upano unit with a minor section of the Cuyuja unit. Finally, Cosanga erodes units similar to Aliso but includes a sliver Agoyán unit.

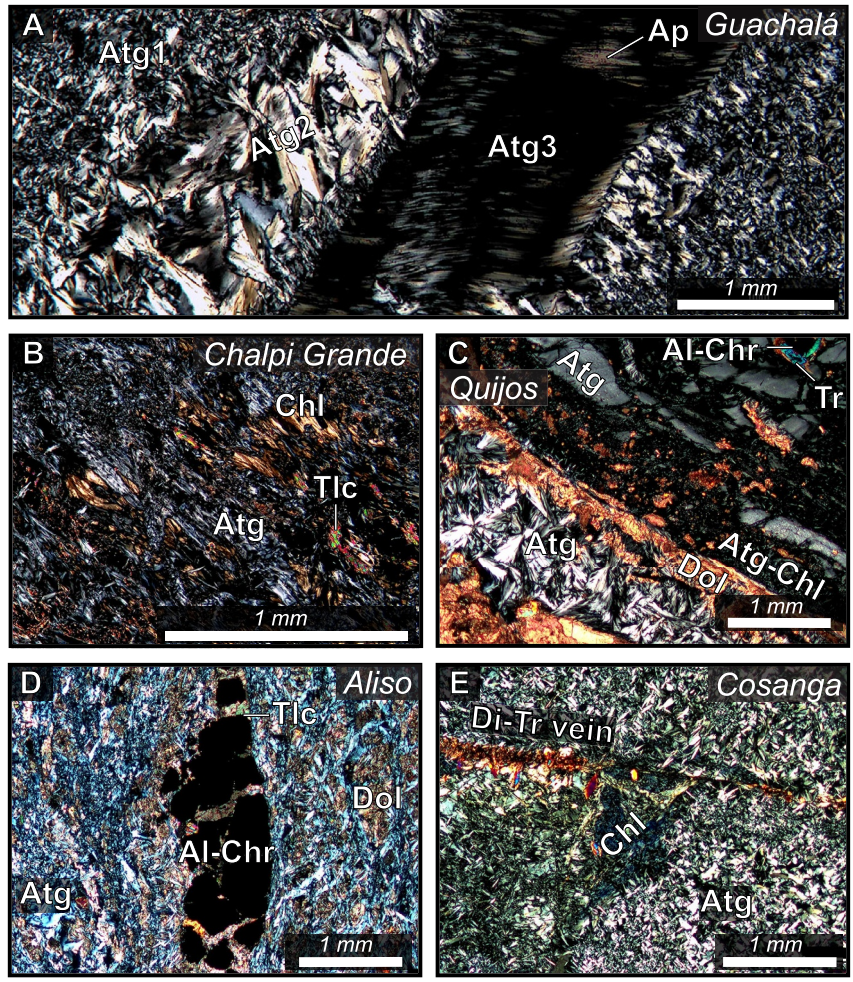

Figure 3. Polarized Light Microscope photographs of the studied serpentinites. (a) Guachalá serpentinite (E16-53-1) with its three generation of antigorite (fine-grained Atg, coarse-grained Atg2, and fibrous Atg3) and apatite (Ap) intergrowth with the fibrous atg3 vein; (b) Serpentinite from Chalpi Grande (E16-7-3) showing replacement of antigorite by brown chlorite and talc; (c) Quijos serpentinite (E16-18-1) showing different occurrences of antigorite, as fibrous, blocky fragments, and coarse-grained veins surrounded by dolomite; (d) Aliso serpentinite (E16-3-1), where dolomite (Dol) and talc (Tlc) overgrow the antigorite, and fill in the spinel (Al-Chr) fractures; (e) Cosanga serpentinite (E16-1-1) with a diopside-tremolite (Di-Tr) vein adjacent to a chlorite (Chl) domain in a medium- to coarse-grained antigorite matrix (Atg).

4.2. Petrology and Mineral Chemistry

Mineral assemblages, PLM photos, compositions, and mineral species interpretations are given in Figures 3–5, Figures S2–S4 in Supporting Information S1, and Data Set S1. All samples are fully serpentinized (Figure 3); antigorite is the main serpentine polymorph and occurs associated with chlorite (Figures 3b, 3c, and 3e, and Figure S5 in Supporting Information S1). Some samples display more than one serpentinization event, preserved as veins and veinlets with different grain sizes relative to the matrix (Figures 3a–3c, and Figure S6 in Supporting Information S1). Two rock textures are dominant and vary depending on the river; Serpentinites from Guachalá, Chalpi Grande, and Cosanga have a massive, homogeneous texture (e.g., Figures S6, S7, S9B, and S9C in Supporting Information S1), whereas those sampled from Quijos and Aliso generally display a well-defined foliation (e.g., Figures S8B, S8C, and S9A in Supporting Information S1). Spinel is ubiquitous in all samples; however, they show varying textures and degrees of alteration between rivers, sometimes obliterating primary features and leaving crystals characterized by sieve-like textures (e.g., Figures S3C and S3D in Supporting Information S1). Other mineral phases include dolomite, minor talc, pyroxene, amphibole, and apatite (Figure 3).

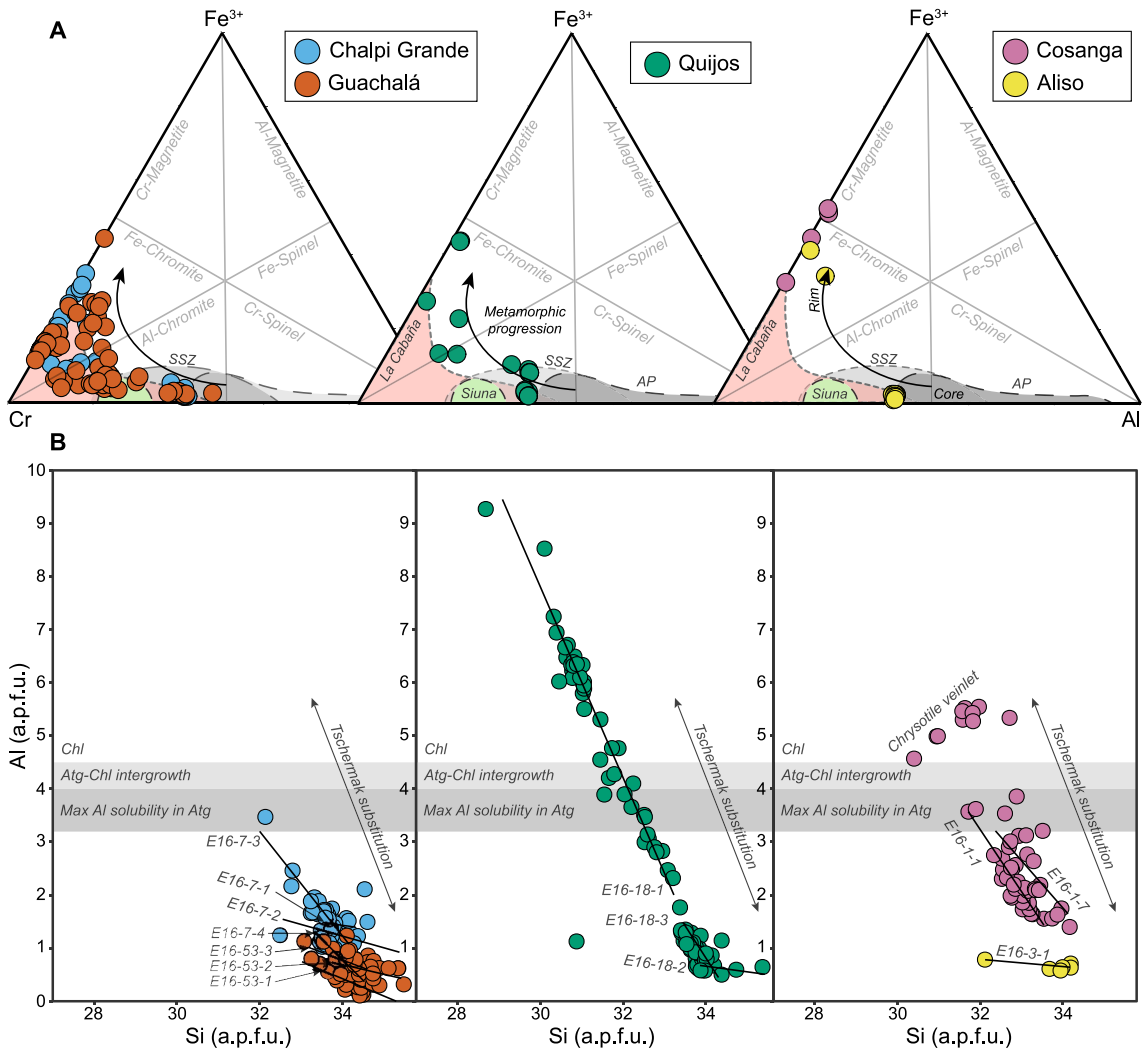

Figure 4. Spinel classification diagrams. (a) Ternary plots for spinel minerals arranged from west (W) to east (E) and based on the location of the rivers and the geological units they drain. SSZ, Supra-subduction zone (Parkinson & Pearce, 1998); AP, Abyssal peridotites (Warren, 2016); Siuna, Siuna Serpentinite Mélange (Flores et al., 2015); La Cabaña metaperidotites (Barra et al., 2014). (b) Mineral chemistry diagrams of antigorite showing trends compatible with Tschermak-type substitution ($Al_2Mg_{-1}Si_{-1}$), dark and light gray bands are based on maximum alumina saturation in antigorite shown in Padrón-Navarta et al. (2013).

Spinel display two main textures with varying preservation of primary/relic features (Figure S3 in Supporting Information S1). The first is characterized by a core-to-rim zonation, where cores are generally Al, Mg-rich, and Fe-poor, while rims are Al-, Mg-poor and Fe-rich (Figures S3A, S3B, and S3D–S3G in Supporting Information S1). This texture is present in all rivers except in Cosanga. The second texture is sieve-like and lacks zonation, although small patches of antigorite or clinochlore have partially replaced the crystal. These spinel grains are heavily depleted in Al and Mg and are only in Chalpi Grande and Cosanga (Figures S3C and S3H in Supporting Information S1). Spinel from Guachalá, Chalpi Grande, and Quijos are associated with or contain inclusions of sulfide (Fe, Fe-Ni, Fe-Ni-Co, and Fe-Ni- Co-As) and Ni-arsenide (Figures S3A and S3C in Supporting Information S1).

Most spinel cores plot in the Al-chromite field, whereas rims, sieve-texture spinel, and depleted cores (e.g., Guachalá, E16-53-1) are Fe-chromite (Figure 4a). #Cr (Cr/Cr + Al) from spinel cores vary from 0.57 to 0.66 (Chalpi Grande, Quijos and Aliso) and 0.52–0.90 (Guachalá). As for #Mg (Mg/Mg + Fe^{2+}), Aliso spinel yielded the highest values of 0.57–0.63, while in Guachalá, Chalpi Grande, and Quijos, it ranges from 0.09 to 0.26 (Figure S4A in Supporting Information S1). Spinel from Cosanga has #Cr and #Mg close to 1.0 and 0.0, respectively. TiO_2 is low overall (0.0–1.0 wt.%) in all rivers, except for sample E16-7-2 from Chalpi Grande, which ranges

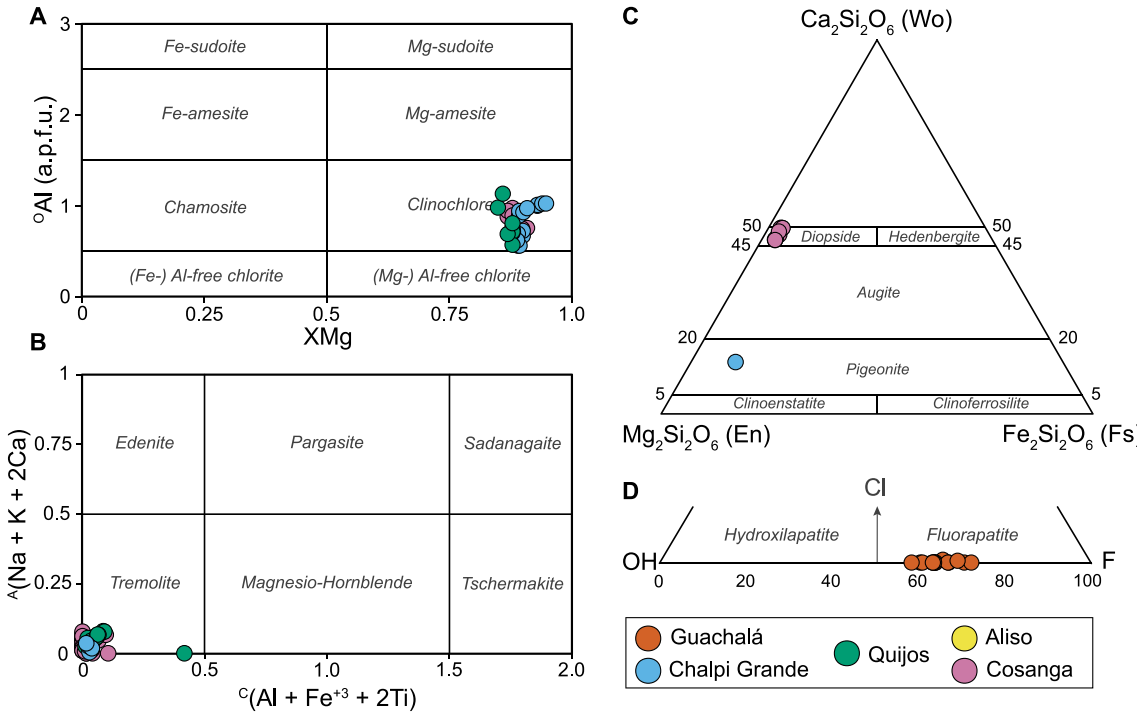

Figure 5. Stoichiometry-based mineral diagrams for (a) Chlorite. (b) Ca-Amphibole. (c) Ca-Mg-Fe-Pyroxene. (d) Apatite.

between 0.5 and 2.3 wt.% in a sieve-like spinel (Figures S4B and S4C in Supporting Information S1). MnO concentrations are generally high in Cosanga (1.4–2.1 wt.%) and Guachalá (1.4–3.5 wt.%) and lower in Chalpi Grande (0.7–1.7 wt.%), Quijos (0.9–1.4 wt.%), and Aliso (0.3–0.7 wt.%). ZnO contents are exceptionally high in Guachalá and Quijos, reaching up to 3.5 wt.%, whereas Chalpi Grande, Aliso, and Cosanga were either below the detection limit or did not exceed 1.6 wt.%.

Serpentine minerals have been characterized by Raman spectroscopy (Figure S5 in Supporting Information S1) on thin sections. Low (0–1,200 cm^{-1}) and high (3,600–3,750 cm^{-1}) wavenumber regions were studied, as these include the lattice vibrational modes and the OH stretching band, respectively (Groppo et al., 2006). Serpentine spectra from each river confirm that antigorite is ubiquitous in matrices and veins, with common peaks in the low wavenumber region at 235, 380 cm^{-1}, a well-defined shoulder in the 550 cm^{-1} region that concludes with a peak at 670, and 1,048 cm^{-1}. The sample from the Aliso River does not have the first peak; this difference is ascribed to dolomite interference, which was identified separately. The high wavenumber region is characterized by a double peak at 3,670 and 3,705 cm^{-1}, present in different intensities depending on the sample (Figure S5 in Supporting Information S1). Late chrysotile veinlets were identified only in sample E16-1-7 (Cosanga) and characterized by peaks at different shifts than antigorite in the low region and a single peak in the high region at c. 3,690 cm^{-1}.

Antigorite chemical analyses suggest variations in SiO_2, MgO, FeO^T, and Al_2O_3 concentrations between rivers. The late chrysotile veinlet of sample E16-1-7 from Cosanga has lower SiO_2 than the antigorite (39.6 ± 1.3 wt.% in Ctl vs. 42.7 ± 0.8 wt.% in Atg) and higher Al_2O_3 (5.6 ± 0.4 wt.% in Ctl vs. 2.5 ± 0.7 wt.% in Atg). Stoichiometry of antigorite from matrices and veins differs between rivers and samples, displaying negative trends between Al and Si in some samples (Figure 4b).

Chlorite minerals were characterized by Raman spectroscopy and EMPA as clinochlore in all samples independent of location (Figure 5a). It occurs as veinlets (Cosanga), spinel rims, and inclusions (Quijos and Cosanga, respectively) and locally replacing antigorite (Chalpi Grande). A chlorite veinlet in Cosanga has an X_{Mg} [Mg/(Fe + Mg)] of 0.90–0.91, compared to the 0.87–0.88 of chlorite of a spinel rim. In Quijos, chlorite X_{Mg} is 0.85–0.88, is found as inclusions in spinel cores and tremolite, and as spinel rims (Figure S3E in Supporting Information S1). The Chalpi Grande chlorite crystals overgrow antigorite and have X_{Mg} values ranging from 0.89 to 0.95.

Amphibole is present as acicular aggregates after antigorite (E16-7-3 Chalpi Grande), spinel and pyroxene overgrowths (E16-1-1 Cosanga; E16-18-1 Quijos), and veins (E16-1-7 Cosanga) (Figures 3b, 3c, and 3e). Based on Hawthorne et al. (2012), all analyses plot in the tremolite field (Figure 5b). Pyroxene (Figure 5c) is present in sample E16-1-1 (Cosanga) as diopside veins ($En_{48}Fs_3Wo_{48}$) based on the pyroxene classification of Morimoto et al. (1988), and is overgrown by tremolite (Figure 3e). In E16-7-3 (Chalpi Grande), small (<10 μm) pyroxene inclusions richer in Fe (6.3% FeO^T) than the diopside measured in Cosanga ($En_{76}Fs_{10}Wo_{14}$) occur within tremolite. However, the total of the analysis is too low and will not be considered for the discussion. Apatite only occurs in E16-53-1 (Guachalá) sample as matrix phenocrysts (up 60 × 50 μm in size), intergrown (up 200 × 60 μm in size) with a fibrous antigorite vein (Figure 3a), or inside porous spinel crystals alongside arsenides (Figure S3A in Supporting Information S1). Analyzed apatite plot in the fluorapatite field, with an average volatile composition of $F_{64.8}Cl_{0.1}OH_{35.1}$ (Figure 5d).

4.3. Major and Trace Element Whole-Rock Chemistry

Whole-rock major and trace element concentrations are reported in Data Set S2. The high volatile content in the studied serpentinites is reflected in the high loss-on-ignition (LOI) values, ranging between 10.4% and 17.4%. SiO_2 and MgO concentrations range from 43.1 to 48.5 wt.% and 38.2 to 43.3 wt.%, respectively. Wide variations are found in Al_2O_3 (1.4–6.5 wt.%) and CaO (0.1–4.5 wt.%), whereas FeO^T is 6.7–9.8 wt.%. A negative correlation exists between LOI and SiO_2 and CaO (Figure S10A in Supporting Information S1). Al_2O_3/SiO_2 ratios range from 0.03 to 0.14, and the MgO/SiO_2 ratios from 0.80 to 0.99 (Figure S10B in Supporting Information S1), all samples follow the terrestrial array, except for samples with high modal chlorite abundance.

Serpentinites rare earth elements (REE) normalized to chondrite (McDonough & Sun, 1995) display relatively flat patterns in all samples, with a slight enrichment in light REE (LREE) and overall depletion in medium to heavy REE (MREE-HREE) (Figure 6a). Multielement spider diagram normalized to primitive mantle (Figure 6b; McDonough & Sun, 1995) shows overall enrichment in fluid mobile elements (FME), particularly high for Sb and As, a moderate enrichment in Cs, and a general enrichment in Pb. Other fluid-mobile elements, such as Rb, Ba, U, and Sr, behave differently; Rb and Ba are generally depleted; U is slightly enriched; and Sr is overall depleted, except in a sample from Chalpi Grande (E16-7-4) and Aliso (E16-3-1), which have high modal abundance of carbonates. High field strength elements (HSFE: Nb, Ta, Zr, Ti) are highly variable. Nb and Ta show moderate enrichments in Chalpi Grande and Guachalá samples and are generally depleted in Quijos, Aliso, and Cosanga. Zr shows values like the primitive mantle, and Ti is overall depleted.

4.4. Geothermobarometry

P-T conditions were estimated for serpentinites from Chalpi Grande (E16-7-3) and Cosanga (E16-1-7). Both samples share the mineral assemblage antigorite ± chlorite overgrown by tremolite ± talc, although chlorite may locally replace antigorite. Whole-rock XRF data of the two serpentinites are nearly identical (Data Set S2); thus, data from sample Chalpi Grande E16-7-3 was used to build the pseudosection (Figure 7a).

Temperature estimates are within the stability range of antigorite but cannot exceed 550–500°C, given the absence of newly formed orthopyroxene or olivine. The Al-in-atg mineral isopleths suggest that serpentinization in Chalpi Grande (E16-7-3) was attained at pressures of 2.5–2.2 GPa. As for Cosanga (E16-1-7), the Al-in-atg contents indicate serpentinization at 1.0–0.6 GPa. The textural features of tremolite indicate growth at a later stage, given its occurrence as coronae in clinopyroxene veins (Cosanga) and spinel (Quijos) or as a replacement of antigorite (Chalpi Grande). Tremolite X_{Mg} is similar in Chalpi Grande and Cosanga (0.940–0.953), and suggests temperatures of 680–660°C. The maximum pressure is inferred in the pseudosection from the amphibole stability field, which at the given temperatures is ∼1.7 GPa. However, the pressure range is between ∼1.5 and 0.5 GPa.

4.5. In-Situ Boron Isotopes and Mineral Trace Elements

In-situ $\delta^{11}B$ values in the serpentinites measured on hydrous minerals, including antigorite, chlorite, and tremolite, are presented in Figure 8. The $\delta^{11}B$ values and mineral trace element (Li, B, Cr, Ni, As, Sr, Y, Sb, Cs, Pb, and U) concentrations are reported in Data Set S3.

The Guachalá samples have overlapping $\delta^{11}B$ values between −4.5 ± 0.6‰ and +1.9 ± 1.0‰. No significant differences were found between matrix and veins (Figure S6 in Supporting Information S1). In Chalpi Grande

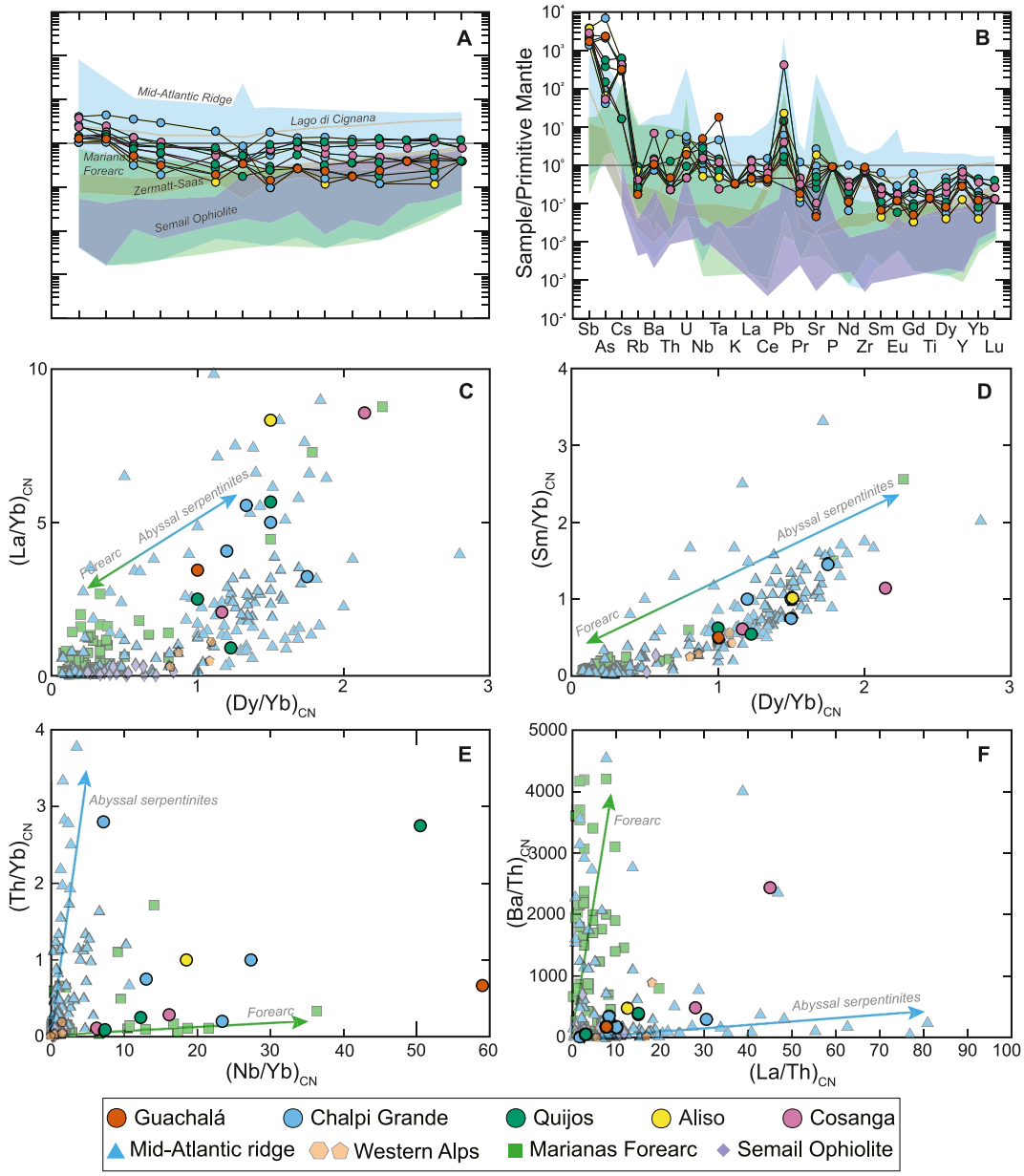

Figure 6. Serpentinite whole-rock trace element data (LA-ICP-MS). (a, b) Chondrite and Primitive Mantle normalized rare earth elements and multielement diagrams. (c, d) Chondrite-normalized $(La/Yb)_{CN}$ versus $(Dy/Yb)_{CN}$ and $(Sm/Yb)_{CN}$ versus $(Dy/Yb)_{CN}$ diagrams. (e, f) $(Th/Yb)_{CN}$ versus $(Nb/Yb)_{CN}$ and $(Ba/Th)_{CN}$ versus $(La/Th)_{CN}$ diagrams. Arrows are interpreted trends followed by forearc and abyssal serpentinites. Shaded fields and data points correspond to serpentinites from Marianas forearc (Parkinson & Pearce, 1998), Alpine serpentinites (Gilio et al., 2019), Mid-Atlantic Ridge (Deschamps et al., 2013), and Semail ophiolite (Hanghøj et al., 2010).

(Figure S7 in Supporting Information S1), the two serpentinites are isotopically homogeneous, with B isotopic compositions between −10.65 ± 0.8‰ and −4.49 ± 1.1‰ and an outlier of −15.87 ± 0.6‰. The Quijos samples display contrasting textures and $\delta^{11}B$ (Figure S8 in Supporting Information S1). Sample E16-18-1 consists of a chaotic mix of dolomite domains within a densely veined antigorite matrix. $\delta^{11}B$ values overlap between veins (−8.3 ± 1.2‰ to −6.2 ± 1.1‰) and matrix (−9.4 ± 1.5‰ to −6.9 ± 1.6‰). Contrarily, E16-18-2 is characterized by foliated bands with significantly different B isotopic compositions. $\delta^{11}B$ ranges from +1.2 ± 0.9 to +5.0 ± 0.6‰, in dark green areas surrounding the black bands; from +1.9 ± 0.3 to +5.7 ± 1.0‰, in white areas (dolomite-rich); from −8.4 ± 0.4 to +0.3 ± 1.3‰, in light green bands; at the contact between dark green and

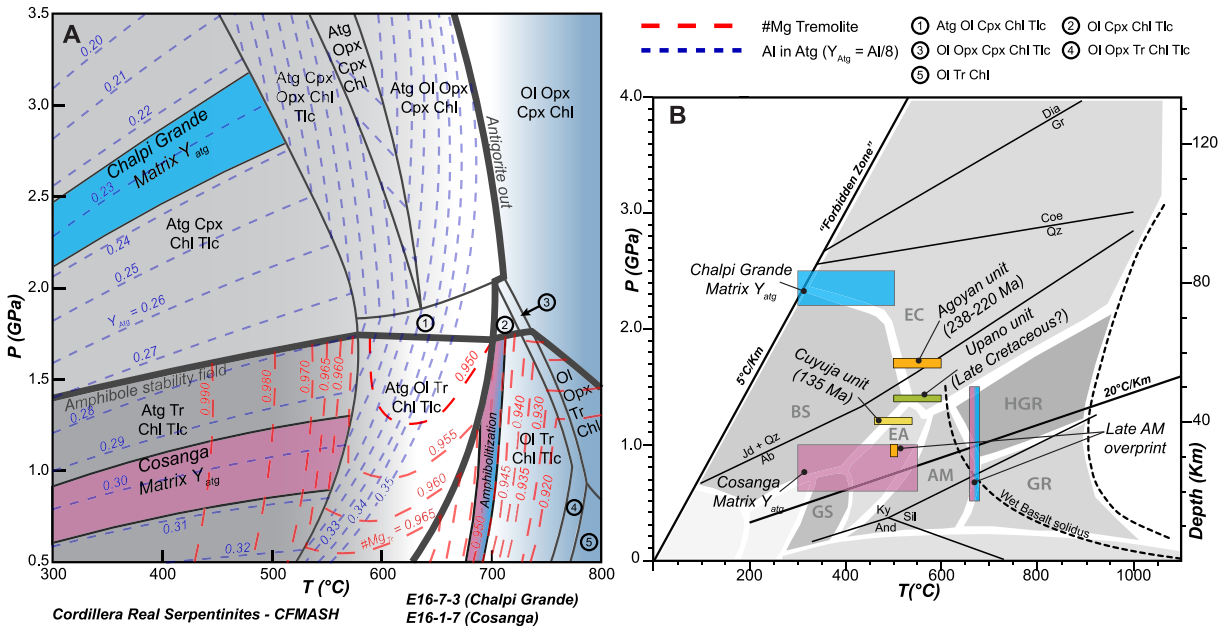

Figure 7. Pressure-Temperature (P-T) estimates of Cordillera Real serpentinites. (a) Water saturated P-T pseudosection for Chalpi Grande (E16-7-3) and Cosanga serpentinites (E16-1-7), using the whole-rock composition of sample E16-7-3 in the CFMASH system. Dashed contours correspond to Al-in-atg contents in blue (Y_{atg} = Al/8) and tremolite X_{Mg} (Mg/(Mg + Fe)) in red. Colored fields in light blue and green represent peak pressures attained by the serpentinites, as well as the interpreted late amphibolitization stage. The thick solid lines represent the predicted amphibole (near horizontal) and antigorite (near vertical) stability fields. (b) P-T diagram showing thermobarometric estimations of Cordillera Real metamorphic subduction-related units. Diagram modified after Flores et al. (2015).

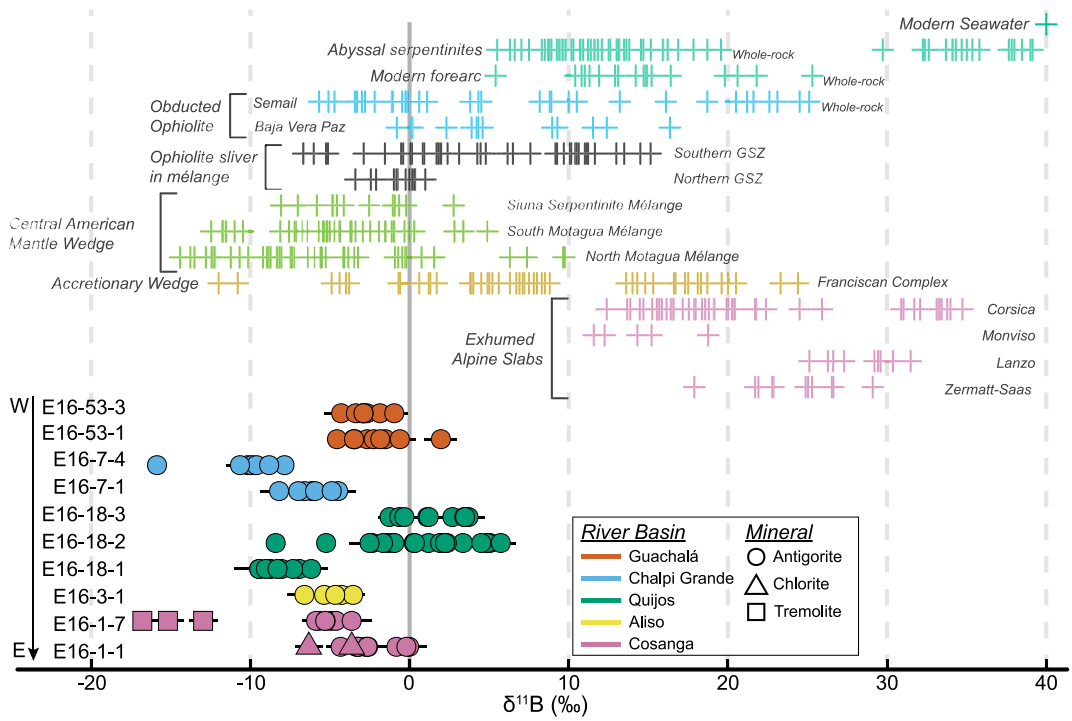

Figure 8. In-situ boron isotope data of Cordillera Real serpentinites compared to published values in modern ocean basins, and exhumed terranes. Published data from C. Boschi et al. (2008, 2013), Harvey et al. (2014), Lécuyer et al. (2002), Martin et al. (2016, 2020, 2023), Prigent et al. (2018), Vils et al. (2009), and Yamada et al. (2019).

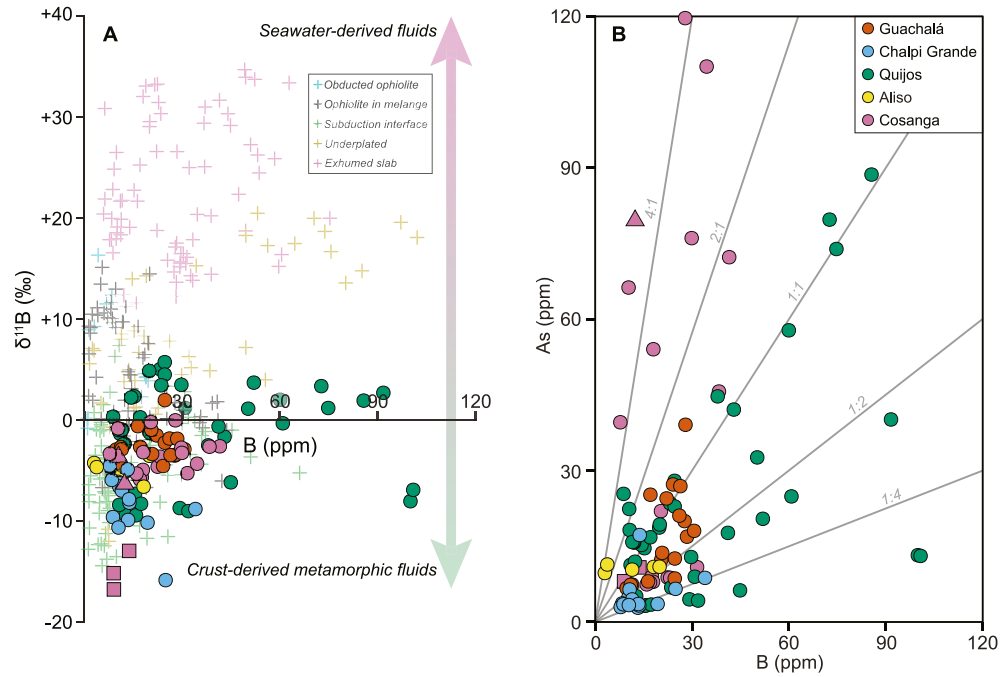

Figure 9. In-situ Boron isotopes and trace element (LA-ICP-MS) data of the studied serpentinites. (a) $\delta^{11}B$ versus B (ppm) concentration, literature in-situ data of exhumed counterparts are from Figure 8. (b) As versus B concentration in measured minerals.

dolomite rich domains from +2.2 ± 0.9 to +4.5 ± 0.6‰; and finally, in green areas (antigorite only), from −2.5 ± 1.3 and +0.3 ± 1.0‰. Sample E16-18-3 also has foliated bands. $\delta^{11}B$ values range from −1.3 ± 0.7 to +1.2 ± 0.8‰ in darker areas (antigorite) and from +2.7 ± 1.2 to +3.7 ± 1.0‰ in lighter green areas (antigorite + talc). The Aliso foliated serpentinite (E16-3-1, Figure S9A in Supporting Information S1) yielded $\delta^{11}B$ values from −6.6 ± 1.0 to −3.5 ± 0.7‰ on antigorite domains interlayered with dolomite bands. Cosanga E16-1-1 sample (Figure S9B in Supporting Information S1) yielded $\delta^{11}B$ values from −4.3 ± 0.9 to −0.03 ± 0.2‰ in the antigorite matrix and from −6.3 ± 0.9 to −3.6 ± 1.0‰ in chlorite (spinel rims). Sample Cosanga E16-1-7 (Figure S9C in Supporting Information S1) has $\delta^{11}B$ values ranging from −5.7 ± 0.6‰ to −3.6 ± 1.3‰ on matrix antigorite, while the tremolite vein yielded values between −16.8 ± 0.2‰ and −12.3 ± 0.9‰.

Boron concentrations range between 3 and 100 ppm for all analyzed areas. In the Guachalá samples, there are minor differences between matrix (20–30 ppm) and vein (c. 11 ppm) B contents (Guachalá E16-53-3), while the apatite-bearing serpentinite Guachalá E16-53-1 shows no variation between the three antigorite generations (16–27 ppm). Among the two analyzed samples, serpentinites from Chalpi Grande have low and overlapping B concentrations of 8–34 ppm. The Quijos serpentinites have the broadest range and highest B contents (9–100 ppm), varying between the serpentine domains analyzed. In Quijos E16-18-1, B concentrations are higher in the matrix (12.7–100.7 ppm, $n = 6$) than in the analyzed veins (15.5–17.3 ppm, $n = 3$). The different bands in Quijos E16-18-2 and E16-18-3 have varying B contents ranging between 8.8 and 85.5 ppm ($n = 21$) and 20.0–91.6 ppm ($n = 9$), respectively. Boron in the Aliso serpentinite has the lowest measured concentration (3–20 ppm). Finally, the Cosanga serpentinites have B values in antigorite of 8–41.5 ppm, whereas chlorite and tremolite generally have lower contents, between 10–12 ppm and 9–13 ppm, respectively. There is no correlation between boron concentration and $\delta^{11}B$ (Figure 9a).

Lithium and Cs concentrations range from 0.4 to 6 ppm and 0.04–0.6 ppm, respectively. In all samples, arsenic displays a broad range between 2.8 and 141 ppm. Serpentinites from Guachalá and Chalpi Grande have overlapping concentrations between their samples (7–40 ppm and 3–17 ppm, respectively). Contrarily, Quijos E16-18-1 has lower As contents than the two counterparts, of 3–13 ppm, versus 12–88 ppm and 7–33 ppm (E16-18-2 and E16-18-3, respectively). The serpentinite from Aliso has comparable As concentrations to Cosanga E16-1-7, between 7.5 and 11 ppm, while Cosanga E16-1-1 yielded the highest overall contents, ranging from 22 to

140 ppm, as well as an outlier spot with 1,056 ppm. A positive correlation exists between measured B and As (Figure 9b), prominent in all serpentinites except for Aliso. Strontium contents are typically below 10 ppm, except in Chalpi Grande E16-7-4 (2–68 ppm) and Aliso E16-3-1 (1–168 ppm). Antimony concentrations are generally low in Guachalá and Chalpi Grande (0.4–1.3 ppm), higher in Quijos E16-18-1, Aliso, and Cosanga (1–11 ppm), and highest in Quijos E16-18-2 and E16-18-3, ranging between 5 and 82 ppm. A positive correlation exists between Sb and B contents (Figure S11 in Supporting Information S1). Lead concentrations show differences in the two Guachalá serpentinites, ranging between 0.05 and 0.16 ppm in E16-53-1 and 0.47–2.6 ppm in E16-53-3. The same is seen in samples from Cosanga, as serpentinite E16-1-1 has antigorite Pb contents ranging from 0.7 to 2 ppm versus 8.5–55.5 ppm in E16-1-7. Lead in chlorite (Cosanga E16-1-1) is higher than the surrounding antigorite (39–87.4 ppm), while tremolite (Cosanga E16-1-7) is lower than the serpentine counterpart, between 3.8 and 11 ppm. In contrast, a consistent Pb range is found in samples from Chalpi Grande, Quijos, and Aliso (0.03–1.7 ppm). Chromium and Ni contents are the highest measured, and while their ranges generally overlap, Cr concentrations are higher, reaching up to 15,000 versus 7,020 ppm of Ni. Yttrium concentrations are overall similar, ranging from 0.1 to 6 ppm, except for Quijos E16-18-1, which has a broader and higher range (0.4–19 ppm).

5. Discussion

5.1. Sources of the Cordillera Real Serpentinites

Watershed delineation analysis for the Guachalá River predicts Devonian to Triassic metamorphic sequences being drained from the distal end of the basin as a potential source of the serpentinites. However, metamorphic rock boulders were scarce at the sampling location, and the serpentinite boulders' relatively large size (~140 × 80 cm) may indicate a proximal source instead. This location is adjacent to the northern section of the Peltetec fault. In the central segment of this major structural feature, serpentinites occur in the Guarguallá River valley (Figure 2) between the Triassic Peltetec ophiolitic belt and the recently described Precambrian-Cambrian Guarguallá mafic-ultramafic unit (Spikings et al., 2021; Villares et al., 2021). Additionally, the boron isotopic signature of the two analyzed serpentinites yields similar results, with an $\delta^{11}B$ range between ~−4.5 and +1.9‰ (Figure 8), resembling serpentinites from ophiolitic slivers within the northern section of the Guatemala Suture Zone (GSZ) (Martin et al., 2023). Thus, the Guachalá serpentinites most likely represent a northward extension of the ultramafic slivers along the Peltetec fault.

The Chalpi Grande drainage basin lithologies suggest that serpentinites are likely sourced from an ultramafic sliver between the Chiguinda and Agoyán units (Figure 2b). The occurrence of Triassic eclogite-facies metapelite boulders alongside serpentinites can be linked to an unmapped ESRMRS body. Watershed analysis of the Quijos River predicts direct erosion of the northern segment of the Quebrada Soledad serpentinite outcrop (Figure 2b). Nevertheless, the morphology, texture, and chemistry of Quijos E16-18-1 differs from the two other samples collected in this river (E16-18-2, E16-18-3). Quijos E16-18-1 was a centimetric and subrounded boulder consisting of a densely veined antigorite matrix and dolomite-rich domains. In contrast, Quijos E16-18-2 and E16-18-3 were collected from metric-sized boulders with well-developed foliation and markedly different serpentine domains (Figures S8B and S8C in Supporting Information S1). The analyzed samples from Chalpi Grande are isotopically similar to Quijos E16-18-1, with values that generally range between ~−10.6 and −4.5‰, similar to Central American mantle wedge serpentinites associated with eclogite and blueschist boulders (Figure 8). Contrarily, the two other serpentinites from Quijos (E16-18-2, E16-18-3) yielded enriched B isotopic signatures, with $\delta^{11}B$ values ranging from ~−2.5 to +5.7‰, which falls within the range of available B isotope data of obducted ophiolites (Figure 8). These results suggest at least two different sources for the Quijos serpentinites, the first one corresponding to the roughly N-S trending Quebrada Soledad serpentinite body, which may extend northward into the Chalpi Grande area (Figure 2b). A second, previously unmapped source likely associated with the other sequences within the Quijos basin, which include epidote-amphibolite-facies metasediments from the Cuyuja unit (Flores et al., 2019).

The proximity between sampling points of the Aliso and Cosanga serpentinites and the adjacent nature of their drainage areas may indicate a common source. However, Litherland et al. (1994) proposed two serpentinite outcrops, one along the Cosanga River in association with the Cretaceous Upano unit and another related to the Urcucocha skarnfield, given the large blocks they reported in neighboring streams. Additionally, there are clear differences in the Aliso and Cosanga serpentinites, particularly the foliated, carbonate-rich nature of the former

versus the massive, diopside-tremolite-bearing assemblage of the latter. Moreover, spinel group minerals from Aliso have a pristine core-to-rim zonation, versus a homogeneous sieve texture found in Cosanga (Figure S3 in Supporting Information S1). Contrarily, the B isotopic signature of the Aliso and Cosanga serpentinites generally overlap in a range between ~−6.6 and 0.0‰, resembling B isotope data of serpentinites from the mantle wedge and some ophiolites in Central America but differing from the Chalpi Grande and Quijos E16-18-1 samples linked to Triassic units (Figure 8). Moreover, preliminary P-T estimations of micaschists from the Upano unit yielded blueschist-eclogite-facies peak conditions, suggesting an association of HP-rocks and serpentinite slivers (Figure 7b). Thus, the serpentinites from Aliso and Cosanga may share a common source linked to the Late Cretaceous Upano unit.

5.2. Metasomatism and Metamorphism of the Cordillera Real Serpentinites

The mineral chemistry of spinel indicates intense alteration during metamorphic processes, as indicated by the core-to-rim zonation and sieve textures (Figure S3 in Supporting Information S1). Only cores from Aliso plot in the overlap between mid-ocean ridge basalt (MORB) or supra subduction fields (Figure 4, Figure S4 in Supporting Information S1). The extent of the alteration and metasomatism is reflected in the loss of Mg and Al and gain of Fe and Ti, similar to La Cabaña in Chile (Barra et al., 2014). Enrichments in Mn and Zn, particularly high in Guachalá and Quijos (up to 3.5 wt.%), have been interpreted to be added by fluid-mediated alteration (Colás et al., 2014). Core-to-rim analyses generally follow a trend toward higher Fe^{3+} proportions relative to Al and Cr (Figure 4). Such a trend has been reported in studies on chromite ores and forearc-mantle serpentinites, compatible with lower-amphibolite facies metamorphism (González-Jiménez et al., 2009; Saumur & Hattori, 2013). Therefore, our findings reveal that spinel minerals in serpentinites record element mobilization and may not be a reliable tool for petrogenetic discrimination, in agreement with the findings of Gamal El Dien et al. (2019), who suggest that these minerals instead give insight into the metasomatism of mantle rocks.

Whole-rock major element discrimination diagrams for the studied serpentinites are inconclusive (Figure S10B in Supporting Information S1). They plot mainly in the abyssal peridotite field, though there is a slight overlap with mantle wedge serpentinites from New Caledonia (Niu, 2004; Raia et al., 2022). The high modal abundance of chlorite in two samples (Quijos E16-18-1; Cosanga E16-1-1) shifts the values in the opposite direction of the terrestrial array due to Al enrichment. Whole-rock trace element data are comparable to serpentinites from the Mid-Atlantic Ridge (MAR), the Marianas forearc, and exhumed Alpine serpentinites from Lago di Cignana, but differ from ophiolite serpentinites (Semail, Oman) and Zermatt-Saas exhumed serpentinites (Figures 6a and 6b). Trace element ratios (Figures 6c–6f) follow trends resembling MAR serpentinites, though a forearc signature is sometimes present (Figures 6e and 6f). Thus, whole-rock chemistry alone cannot explain the tectonic setting of the Cordillera Real serpentinite protoliths, as it yields mixed results between an abyssal and a forearc origin.

The observed enrichments in certain fluid-mobile elements (Sb, As, Cs, Figure 6b) have been associated with the addition of sediment- or seawater-derived fluids during serpentinization (Lafay et al., 2013; Peters et al., 2017) or with the lizardite-antigorite transition in participation with sediment-derived fluids (Deschamps et al., 2013; Wu et al., 2021), while the depletion in whole-rock Rb, Sr, and Ba is also linked to this transition (Pettke & Bretscher, 2022). Mineral trace element data agree with the enrichments found in whole-rock analyses, where there is a positive correlation between B and Sb, As, and Cs, indicating that the serpentinizing fluid in the studied samples was rich in these FME (Figure 9b, Figure S11 in Supporting Information S1).

The metasomatic event responsible for the serpentinization of the Cordillera Real samples is preserved in the B isotopic signature (Figures 8 and 9). The two Guachalá samples have a consistent signature with overlapping $\delta^{11}B$ values (−4.6 to −0.6‰), suggesting a common origin of the fluid responsible for serpentinization. The two samples from Chalpi Grande and E16-18-1 from Quijos display a more negative signature ranging from −10.6‰ to −4.5‰ (the outlier data point at −15.9 ± 0.6‰ in Chalpi Grande E16-7-4 is not taken into account in this discussion), indicating serpentinization by a similar crust-derived fluid. The two other samples from Quijos have highly variable $\delta^{11}B$, trending toward positive values, depending on the antigorite domain considered. In E16-18-2, the two highly negative outliers will not be considered in the discussion, as they are close to dolomite domains, and B isotopes in carbonates calibrated with NIST SRM 612 are known to yield inexact, strongly negative values (K. A. Evans & Frost, 2021; Sadekov et al., 2019). The other antigorite domains in this sample and sample E16-18-3 are mildly negative to slightly positive ($\delta^{11}B$ between ~+1 and +6‰) in domains where antigorite is mixed with other minerals (talc or spinel and sulfide, and $\delta^{11}B$ between ~−2.5 and +1‰ in antigorite-only domains).

This may indicate that the different domains formed from successive fluids or that the minerals added to the domains shifted the B isotopic signature toward slightly positive values. These variable $\delta^{11}B$ values have been documented on serpentinites from ophiolitic sequences, in which a mixture of seawater-derived and subducted crust-derived fluid is responsible for serpentinization (Lécuyer et al., 2002; Martin et al., 2016, 2023; Prigent et al., 2018). In the case of Aliso and Cosanga, overlapping antigorite $\delta^{11}B$ values indicate serpentinization by similar metamorphic fluids, likely pointing to a common outcrop source. The intense spinel alteration of Cosanga can be ascribed to late events, potentially linked to the diopside-tremolite veins. Contrarily, spinel from Aliso did not undergo significant alteration, as indicated by pristine cores. In-situ B isotopic signatures in serpentinites are mostly negative, suggesting serpentinization by crust-derived metamorphic fluids for all samples with none or negligible seawater influence.

The ubiquity of antigorite and the absence of secondary olivine or orthopyroxene (dehydration products of serpentine) in all samples indicate that serpentinization took place within the antigorite stability field, between c. 300 and 620–680°C, depending on the aluminum content (B. W. Evans, 2004; Padrón-Navarta et al., 2010). The lack of Tschermak-type substitution in antigorite and amphibole in samples from Guachalá and Aliso does not allow us to estimate P-T conditions. However, the temperatures can be assumed to be within the antigorite stability range. Further constraints on the metamorphic history of the Cordillera Real serpentinites, as calculated for samples from Chalpi Grande and Cosanga, reveal an initial stage of high-temperature serpentinization, and a subsequent amphibolitization stage indicated by the growth of tremolite (Figure 7a). In Chalpi Grande, serpentinization was attained at pressures of 2.5–2.2 GPa, and temperatures that did not exceed 500°C. This is compatible with eclogite facies conditions, which have also been reported in outcrops and boulders of Triassic metapelites from the Agoyán unit that underwent peak metamorphic conditions of 1.7 ± 0.2 GPa and 550 ± 50°C, and a subsequent retrograde stage at 1–0.9 GPa and 500°C (Figure 7b), under epidote-amphibolite facies (Flores et al., 2019). Even though thermodynamic modeling was not possible in any of the ophiolitic samples of Quijos (E16-18-2, E16-18-3), rough temperature estimates are within the stability field of antigorite without antigorite breakdown products. Further, these blocks occur near outcrops of the Cuyuja unit, where epidote-amphibolite-facies garnet-metapelites yielded metamorphic peak conditions of 1.2 ± 0.1 GPa and 500 ± 40°C (Figure 7b), and contain metamorphic zircons of ∼135 Ma (Flores et al., 2019). In the Cosanga serpentinites, serpentinization occurred at pressures of 1.0–0.6 GPa and temperatures that did not exceed 550°C, suggesting metamorphic facies conditions varying from upper greenschist, blueschist, to epidote-amphibolite. Contrastingly, mica-bearing mafic schist from the Late Cretaceous Upano unit yielded higher peak metamorphic conditions of ∼1.4 GPa and 600–500°C, at blueschist-eclogite facies (Donoso-Tapia et al., 2022).

Our findings show that the Cordillera Real serpentinization was driven by crustal related fluids, and P-T conditions suggest the exhumation of various ultramafic, pelitic, and metamafic slivers from depths varying from ∼80 to 30 km during the Triassic and Late Cretaceous (Figure 7b). These conditions are compatible with subduction zone tectonic settings, either in a forearc environment, or short-lived subduction stages during back-arc basin closure, where exhumation of HP-LT slivers or obduction of ophiolitic sequences commonly occur.

5.3. The Role of Serpentinites in the Evolution of Non-Collisional Orogens

The complex history of exhumed serpentinite slivers in the non-collisional paleo-Andean orogen appears to be closely related to extensional-compressional cycles (Figure 1). The oldest evidence of extension is found in the southern Andes, within the Eastern Andean Metamorphic Complex (EAMC), composed of mafic-ultramafic sequences and serpentinites interpreted as an exhumed portion of Carboniferous oceanic crust from a marginal basin (Rojo et al., 2021). The EAMC may record the first extensional phase following the amalgamation of Western Gondwana during Devonian-Carboniferous times. In addition, the Devonian-Carboniferous metasediments of the Cordillera Real (Chiguinda unit) have been suggested to have been deposited in a back-arc basin. However, it is unknown whether new oceanic lithosphere was formed (Spikings et al., 2021). North of the EAMC, the Bahia Mansa Metamorphic Complex (BMMC) contains several discrete serpentinite bodies associated with pelitic and mafic schists that attained peak metamorphic conditions at blueschist to amphibolite-eclogite facies (Duhart & Adriasola, 2008; Duhart et al., 2001; Hervé, 1988; Kato et al., 2008; Willner et al., 2009). Enclosed in the BMMC, the La Cabaña ultramafic bodies consist of serpentinized metaperidotites, chromitites, and metagabbros embedded in a mylonitic antigorite-serpentinite matrix. The metaperidotites reached peak conditions up to 2.5 GPa and 600°C, while a zircon U-Pb age from a chromitite yielded 287 Ma (González-Jiménez et al., 2017; Romero et al., 2018). Recent petrological and geophysical studies in this unit suggest that it corresponds to a

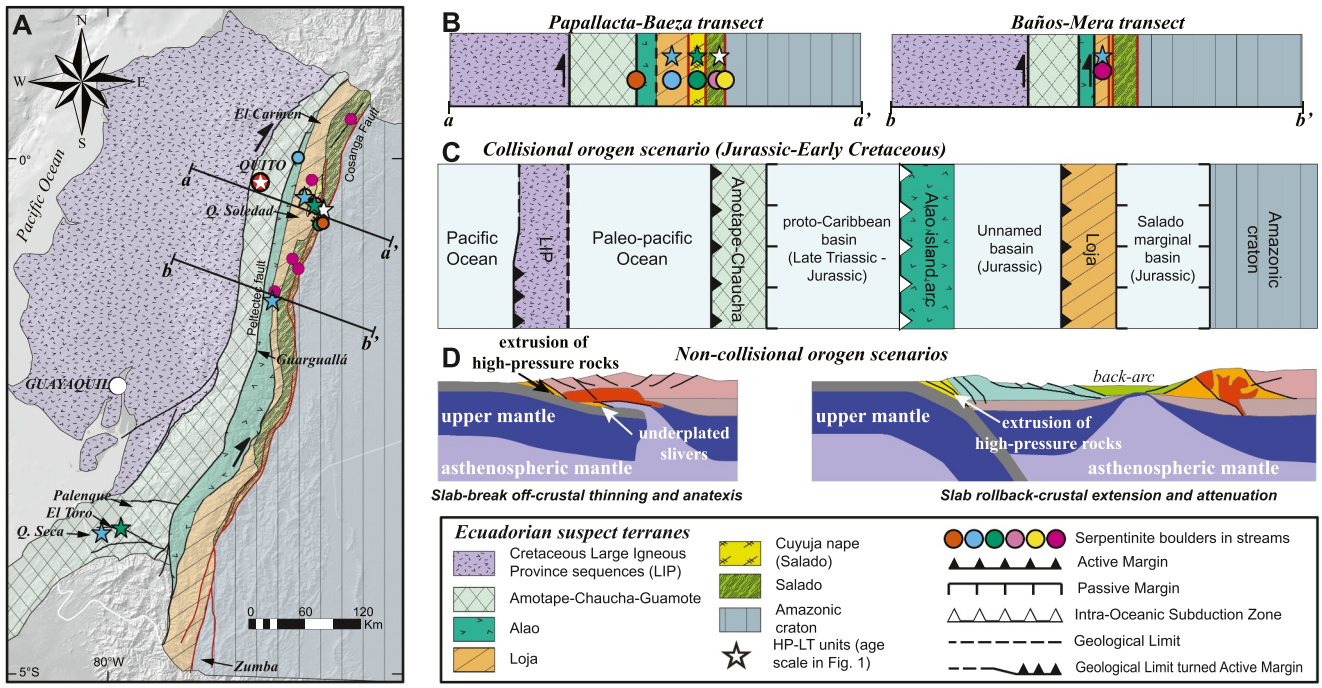

Figure 10. Tectonic scenarios for the evolution of the northern Andes in the Cordillera Real segment. (a, b) Proposed suspect terranes in Ecuador and their current architecture in two transects along the central Cordillera Real. The position of the samples relative to the terranes is tentative based on the watershed delineation analysis. (c) Collisional orogen scenario as proposed by Litherland et al. (1994). (d) Non-collisional orogen tectonic scenarios for the northern Andes, modified after Cochrane et al. (2014b) and Riel et al. (2013).

portion of the oceanic mantle incorporated into the subduction interface along with metasediments prior to their exhumation (Plissart et al., 2019; Sanhueza et al., 2022). No Permian HP–LT metamorphism associated with serpentinites has been reported in the northern Andes.

The first comprehensive study on the evolution of Ecuador suggests a collisional model involving multiple terranes (Litherland et al., 1994). The latter proposed seven possible fault-bounded terranes (Figures 10a and 10b). In this model, the Amotape-Chaucha terranes were separated from the Loja-Amazonic craton during the opening of the proto-Caribbean basin in the Jurassic. Guamote represents the passive margin of Amotape-Chaucha, while Loja was the active margin rifted from the Amazonic craton by the opening of the Salado marginal depocenter. The oceanic basin between the proto-Caribbean spreading center axis and the Loja active margin encloses an island arc called Alao. The closure of the three basins (Figure 10c) is related to a single collisional event at c. 135 Ma, marked in the Peltetec suture and the Cordillera Real stack of overthrusted slivers (Figure 10b). A subsequent collision of the exotic LIP fragment occurred in the Late Cretaceous-Paleocene. This collisional model implies at least three potential sources for the Cordillera Real serpentinites linked to the closure of the aforementioned basins. This scenario would require a coeval metamorphic event. In contrast, peak metamorphic ages for the Agoyán (~235 Ma), Cuyuja (~135 Ma), and potentially Upano unit (Late Cretaceous-Paleocene) argue for at least three events. Additionally, new radiometric data in the Peltetec ophiolitic belt yielded a zircon U-Pb crystallization age of ~228 Ma, different from the c. 135 Ma (Ar-Ar on plagioclase) initially proposed for this possible suture zone (Spikings et al., 2015; Villares et al., 2021).

Contrarily, an autochthonous, non-collisional origin for the Cordillera Real high-grade metamorphic units was proposed based on similar stratigraphic and structural observations on either side of the mountain belt and across the assumed terranes boundaries (Pratt et al., 2005). The large abundance of mafic volcanic sequences with arc or ophiolitic affinities was the main argument for the collisional model (Litherland et al., 1994). However, Triassic mafic rocks in Ecuador and Colombia (e.g., Piedras, Peltetec, Monte Olivo, Santa Elena, Aburrá) have been linked to widespread peraluminous granites and migmatites (e.g., Moromoro, Sabanillas, Tres Lagunas, Cajamarca) formed from slab breakoff/crustal thinning and anatexis in the Ecuadorian Amotape block, or trench retreat and slab rollback in the Cordillera Real domain during eastward migration of South America caused by

rifting during the Pangea continental break up (Cochrane et al., 2014a; Riel et al., 2013; Villares et al., 2021). In the northern Colombian Andes, serpentinites within the Medellín metaharzburguitic unit have been associated with the Triassic Aburrá ophiolite and interpreted as a fragment of oceanic lithospheric mantle formed at a back-arc basin (Garcia-Casco et al., 2020; Ibañez-Mejia et al., 2020). In the slab breakoff scenario, the Triassic mafic metamorphic sequences, mafic blueschists, and ultramafic slivers from the Piedras and Arenillas-Panupalí units of the Amotape block were interpreted as exhumation of mafic lower crust and underplated oceanic crust (Figure 10d). However, in this similar scenario, exhumation of subduction-related metamorphic rocks has also been suggested to occur by extrusion of metamorphic slivers along major thrust faults in the forearc (e.g., Duretz et al., 2011, 2012). Additionally, in the slab rollback scenario, the relative divergence between the downgoing slab and the upper plate can create the space or reduce the downgoing shear stress and enhance exhumation in the forearc (Brun & Faccenna, 2008). The back-arc tectonic scenario suggested for the Peltetec ophiolitic belt (Villares et al., 2021) can also be extended to other Triassic mafic-ultramafic complexes within the Cordillera Real (Zumba, Monte Olivo). In this context, the Quebrada Soledad serpentinites and the Agoyán metapelites should represent exhumed slivers along the forearc.

Another regional slab rollback phase in the northern Andes has been proposed during the Late Jurassic-Early Cretaceous (e.g., Braz et al., 2018; Cochrane et al., 2014b). This phase resulted in crustal extension, arc migration, and formation of oceanic lithosphere in Colombia and Ecuador (Figure 10d). Westward migration of South America due to the opening of the Central Atlantic closed these basins c. 115–105 Ma. As a result, two discontinuous ESRMRS belts were formed, one in the western margin of the northern Andes and the other in the eastern margin, interpreted as the Cosanga Fault (Cochrane et al., 2014b). In Colombia, two HP–LT sequences and associated serpentinite parallel belts in Central Cordillera's western and eastern margins have also been reported. The western Pijao and Barragán units (c. 129–120 Ma) are interpreted as being exhumed during slab rollback in the forearc (Avellaneda-Jiménez et al., 2022; A. Bustamante et al., 2012; García-Ramírez et al., 2017). Comparable peak and exhumation ages were obtained in the ∼133–114 Ma Amotape block Raspas Complex (D. Bosch et al., 2002; Gabriele, 2002; John et al., 2010), interpreted as an exhumed complete slab segment associated with subducted seamounts. In the eastern HP–LT belt in the Colombia Central Cordillera, the ∼68–55 Ma Jambaló unit has been described in association with serpentinized peridotites exhumed during back-arc closure (C. Bustamante & Bustamante, 2019; A. Bustamante et al., 2011, 2021). Recently discovered blueschist-eclogite-facies metapelites and potential serpentinite slivers of the Upano unit might represent Late Cretaceous-Paleocene counterparts in the Ecuadorian Cordillera Real (Donoso-Tapia et al., 2022).

Cretaceous ESRMRS in southern Chile (Diego de Almagro, Cordillera Darwin, Rocas Verdes basin) share similar metamorphic ages and tectonic scenarios. Nevertheless serpentinites have not been reported. In the 132–75 Ma Diego de Almagro complex, underplated stacks of tectonic slivers escaped subduction and traveled through the forearc by forced return flow, though extensional-compressional phases were not proposed as a driving mechanism (Angiboust et al., 2017, 2018; Hyppolito et al., 2016). In contrast, the Rocas Verdes basin and the Cordillera Darwin complexes contain amphibolite-facies metasediments and metamafic rocks formed in an extensional phase, that subsequently, recorded a 87–60 Ma obduction and underthrusting after a short-lived subduction phase during back-arc closure (Grunow et al., 1992; Klepeis et al., 2010; Kohn et al., 1995).

Recently, Faccenna et al. (2021) proposed that 10–100 Myr orogenic cycles with distinct periods of subduction style control the deformation in the upper plate, changing from extension during trench retreat (slab pull orogeny) and compression during slab anchoring in the lower mantle (slab suction orogeny), which is the stage of the modern Andes. Exhumation of HP rocks in the forearc region is known to be enhanced by extensional phases due to slab rollback (Brun & Faccenna, 2008). As described above, slab rollback-related extension has been recorded in the northern Andes during the Triassic and Jurassic-Early Cretaceous. This likely resulted in the extrusion of metamorphic slivers along major faults in the forearc and opening of back-arc basins subsequently closed during compressional phases, favoring ophiolite obduction and metamorphic rocks exhumation in the back-arc related suture.

6. Conclusions

Our data allow us to distinguish four serpentinite slivers being drained into the Cordillera Real rivers. These slivers are associated with Precambrian-Cambrian or Triassic mafic-ultramafic sequences along the Peltetec Fault (Guachalá), Triassic metamorphic sequences associated with the Agoyán unit and Quebrada Soledad serpentinite

body (Chalpi Grande/Quijos E16-18-1), possibly Jurassic-Early Cretaceous blueschist—epidote-amphibolite facies metapelites of the Cuyuja unit (Quijos E16-18-2, E16-18-3), and Late Cretaceous-Paleocene blueschist to eclogite-facies metamafic and metasedimentary sequences from the Upano unit (Aliso and Cosanga). Antigorite is ubiquitous in all serpentinites, and spinel is the only preserved protolith phase. Spinel chemistry and whole-rock data are inconclusive to distinguish protolith sources; instead, they suggest a rich metasomatic history. In contrast, FME and in-situ boron isotope data indicate that serpentinization was driven by crust-derived metamorphic fluids in a subduction zone setting, either in the mantle wedge or associated with obducted ophiolites. Thermodynamic modeling indicates serpentinization at eclogite and upper greenschist, blueschist to epidote-amphibolite-facies in Chalpi Grande and Cosanga, respectively. A subsequent late amphibolitization event is recorded in both localities and the Quijos E16-18-1 sample.

Recently obtained metamorphic ages disagree with the proposed single collisional model for the evolution of the Cordillera Real and the northern Andes. Instead, a non-collisional model characterized by regional extensional and compressional phases is favored due to the widespread occurrence of similar paleo-Andean lithologies along the orogen. The origin of these complexes has been linked to regional extensional phases driven by slab rollback that favored exhumation of HP-LT metamorphic slivers into the forearc and triggered the opening of mafic-floored back-arc basins. Inversion of back-arc basins during compressional phases culminated with ophiolite obduction and associated HP-LT metamorphic rock exhumation. This non-collisional model is in line with recently proposed 10–100 Ma extensional-compressional cycles in orogenic belts.

Data Availability Statement

Supplementary figures and data generated in this study are included in Supporting Information S1 and Data Sets S1–S3. Data Sets related to this article can be found at EarthChem Library—Repository (Donoso-Tapia et al., 2024), an open-source online data repository for geochemical datasets.

Acknowledgments
This study was supported by the US National Science Foundation EAR 2150618 to K.E.F and EAR 1951166 to C. M. The authors thank the helpful assistance of Kyle Dayton (Cornell), Lyndsey Fisher (Cornell), and Louise Bolge (LDEO), with the Raman, LA-ICP-MS, and LA-MC-ICP-MS facilities, respectively. DDT thanks Daniel N. Goldman (UNC), Clément Herviou (UNC), Drew Coleman (UNC), and George E. Harlow (AMNH) for their valuable discussion and input. We are grateful for insightful suggestions from Fabian Villares and an anonymous reviewer that enhanced the manuscript.

References

Agard, P., Yamato, P., Jolivet, L., & Burov, E. (2009). Exhumation of oceanic blueschists and eclogites in subduction zones: Timing and mechanisms. *Earth-Science Reviews*, *92*(1), 53–79. https://doi.org/10.1016/j.earscirev.2008.11.002

Agard, P., Zuo, X., Funiciello, F., Bellahsen, N., Faccenna, C., & Savva, D. (2014). Obduction: Why, how and where. Clues from analog models. *Earth and Planetary Science Letters*, *393*, 132–145. https://doi.org/10.1016/j.epsl.2014.02.021

Alt, J. C., Garrido, C. J., Shanks, W. C., Turchyn, A., Padrón-Navarta, J. A., López Sánchez-Vizcaíno, V., et al. (2012). Recycling of water, carbon, and sulfur during subduction of serpentinites: A stable isotope study of Cerro del Almirez, Spain. *Earth and Planetary Science Letters*, *327–328*, 50–60. https://doi.org/10.1016/j.epsl.2012.01.029

Angiboust, S., Cambeses, A., Hyppolito, T., Glodny, J., Monié, P., Calderón, M., & Juliani, C. (2018). A 100-m.y.-long window onto mass-flow processes in the Patagonian Mesozoic subduction zone (Diego de Almagro Island, Chile). *GSA Bulletin*, *130*(9–10), 1439–1456. https://doi.org/10.1130/B31891.1

Angiboust, S., Hyppolito, T., Glodny, J., Cambeses, A., Garcia-Casco, A., Calderón, M., & Juliani, C. (2017). Hot subduction in the middle Jurassic and partial melting of oceanic crust in Chilean Patagonia. *Gondwana Research*, *42*, 104–125. https://doi.org/10.1016/j.gr.2016.10.007

Aspden, J. A., Bonilla, W., & Duque, P. (1995). *The El Oro metamorphic complex, Ecuador: Geology and economic mineral deposits*. British Geological Survey.

Aspden, J. A., & Litherland, M. (1992). The geology and Mesozoic collisional history of the Cordillera Real, Ecuador. *Tectonophysics*, *205*(1), 187–204. https://doi.org/10.1016/0040-1951(92)90426-7

Avellaneda-Jiménez, D. S., Cardona, A., Valencia, V., León, S., & Blanco-Quintero, I. F. (2022). Metamorphic gradient modification in the Early Cretaceous Northern Andes subduction zone: A record from thermally overprinted high-pressure rocks. *Geoscience Frontiers*, *13*(2), 101090. https://doi.org/10.1016/j.gsf.2020.09.019

Barra, F., Gervilla, F., Hernández, E., Reich, M., Padrón-Navarta, J. A., & González-Jiménez, J. M. (2014). Alteration patterns of chromian spinels from La Cabaña peridotite, south-central Chile. *Mineralogy and Petrology*, *108*(6), 819–836. https://doi.org/10.1007/s00710-014-0335-5

Bocchio, R., De Capitani, L., Liborio, G., Maresch, W. V., & Mottana, A. (1996). Equilibration conditions of eclogite lenses from Isla Margarita, Venezuela: Implications for the tectonic evolution of the metasedimentary Juan Griego Group. *Lithos*, *37*(1), 39–59. https://doi.org/10.1016/0024-4937(95)00014-3

Bosch, D., Gabriele, P., Lapierre, H., Malfere, J.-L., & Jaillard, E. (2002). Geodynamic significance of the Raspas Metamorphic Complex (SW Ecuador): Geochemical and isotopic constraints. *Tectonophysics*, *345*(1), 83–102. https://doi.org/10.1016/S0040-1951(01)00207-4

Boschi, C., Bonatti, E., Ligi, M., Brunelli, D., Cipriani, A., Dallai, L., et al. (2013). Serpentinization of mantle peridotites along an uplifted lithospheric section, Mid Atlantic Ridge at 11° N. *Lithos*, *178*, 3–23. https://doi.org/10.1016/j.lithos.2013.06.003

Boschi, C., Dini, A., Früh-Green, G. L., & Kelley, D. S. (2008). Isotopic and element exchange during serpentinization and metasomatism at the Atlantis Massif (MAR 30°N): Insights from B and Sr isotope data. *Geochimica et Cosmochimica Acta*, *72*(7), 1801–1823. https://doi.org/10.1016/j.gca.2008.01.013

Braz, C., Seton, M., Flament, N., & Müller, R. D. (2018). Geodynamic reconstruction of an accreted Cretaceous back-arc basin in the Northern Andes. *Journal of Geodynamics*, *121*, 115–132. https://doi.org/10.1016/j.jog.2018.09.008

Brook, M. (1984). New radiometric age data from SW Colombia: Cali, Colombia (Vol. *10*). https://doi.org/10.1144/gsjgs.141.5.0831

Brun, J.-P., & Faccenna, C. (2008). Exhumation of high-pressure rocks driven by slab rollback. *Earth and Planetary Science Letters*, *272*(1), 1–7. https://doi.org/10.1016/j.epsl.2008.02.038

Bustamante, A. (2008). *Geotermobarometria, geoquímica, geocronologia e evolução tectônica das rochas da fácies xisto azul nas áreas de Jambaló (Cauca) e Barragán (Valle del Cauca)*. Universidade de São Paulo.

Bustamante, A., Bustamante, C., Cardona, A., Juliani, C., & Pereira da Silva, S. (2021). Jambaló blueschist and greenschist protoliths in the Central Cordillera of the Colombian Andes and their tectonic implications for Late Cretaceous Caribbean-South American interactions. *Journal of South American Earth Sciences*, *107*, 102977. https://doi.org/10.1016/j.jsames.2020.102977

Bustamante, A., Juliani, C., Essene, E. J., Hall, C. M., & Hyppolito, T. (2012). Geochemical constraints on blueschist- and amphibolite-facies rocks of the Central Cordillera of Colombia: The Andean Barragán region. *International Geology Review*, *54*(9), 1013–1030. https://doi.org/10.1080/00206814.2011.594226

Bustamante, A., Juliani, C., Hall, C. M., & Essene, E. J. (2011). $^{40}Ar/^{39}Ar$ ages from blueschists of the Jambaló region, Central Cordillera of Colombia: Implications on the styles of accretion in the Northern Andes. *Geológica Acta*, *9*(3–4), 351–362. https://doi.org/10.1344/105.000001697

Bustamante, C., & Bustamante, A. (2019). Two Cretaceous subduction events in the Central Cordillera: Insights from the high P–low T metamorphism. In J. Gómez & A. O. Pinilla–Pachon (Eds.), *The geology of Colombia, Volume 2 Mesozoic* (Vol. 36, pp. 485–498). Servicio Geológico Colombiano, Publicaciones Geológicas Especiales. https://doi.org/10.32685/pub.esp.36.2019.02

Butjosa, L., Cambeses, A., Proenza, J. A., Blanco-Quintero, I. F., Agostini, S., Iturralde-Vinent, M. A., & Garcia-Casco, A. (2023). Fluid flow in the subduction channel: Tremolite veins and associated blackwalls in antigoritite (Villa Clara serpentinite mélange, Cuba). *Lithos*, *436–437*, 106973. https://doi.org/10.1016/j.lithos.2022.106973

Casquet, C., Baldo, E., Pankhurst, R. J., Rapela, C. W., Galindo, C., Fanning, C. M., & Saavedra, J. (2001). Involvement of the Argentine Precordillera terrane in the Famatinian mobile belt: U-Pb SHRIMP and metamorphic evidence from the Sierra de Pie de Palo. *Geology*, *29*(8), 703–706. https://doi.org/10.1130/0091-7613(2001)029<0703:IOTAPT>2.0.CO;2

Cawood, P. A., Kröner, A., Collins, W. J., Kusky, T. M., Mooney, W. D., & Windley, B. F. (2009). Accretionary orogens through Earth history. *Geological Society, London, Special Publications*, *318*(1), 1–36. https://doi.org/10.1144/SP318.1

Chiaradia, M., Vallance, J., Fontboté, L., Stein, H., Schaltegger, U., Coder, J., et al. (2008). U–Pb, Re–Os, and $^{40}Ar/_{39}Ar$ geochronology of the Nambija Au-skarn and Pangui porphyry Cu deposits, Ecuador: Implications for the Jurassic metallogenic belt of the Northern Andes. *Mineralium Deposita*, *44*(4), 371–387. https://doi.org/10.1007/s00126-008-0210-6

Cochrane, R., Spikings, R., Gerdes, A., Ulianov, A., Mora, A., Villagómez, D., et al. (2014a). Permo-Triassic anatexis, continental rifting and the disassembly of western Pangaea. *Lithos*, *190–191*, 383–402. https://doi.org/10.1016/j.lithos.2013.12.020

Cochrane, R., Spikings, R., Gerdes, A., Winkler, W., Ulianov, A., Mora, A., & Chiaradia, M. (2014b). Distinguishing between in-situ and accretionary growth of continents along active margins. *Lithos*, *202–203*, 382–394. https://doi.org/10.1016/j.lithos.2014.05.031

Colás, V., González-Jiménez, J. M., Griffin, W. L., Fanlo, I., Gervilla, F., O'Reilly, S. Y., et al. (2014). Fingerprints of metamorphism in chromite: New insights from minor and trace elements. *Chemical Geology*, *389*, 137–152. https://doi.org/10.1016/j.chemgeo.2014.10.001

Connolly, J. A. D. (2005). Computation of phase equilibria by linear programming: A tool for geodynamic modeling and its application to subduction zone decarbonation. *Earth and Planetary Science Letters*, *236*(1), 524–541. https://doi.org/10.1016/j.epsl.2005.04.033

Davis, J. S., Roeske, S. M., McClelland, W. C., & Snee, L. W. (1999). Closing the ocean between the Precordillera terrane and Chilenia: Early Devonian ophiolite emplacement and deformation in the southwest Precordillera Laurentia-Gondwana connections before Pangea. In V. A. Ramos & J. D. Keppie (Eds.), *Special papers* (Vol. 336, p. 0). Geological Society of America. https://doi.org/10.1130/0-8137-2336-1.115

Deschamps, F., Godard, M., Guillot, S., & Hattori, K. (2013). Geochemistry of subduction zone serpentinites: A review. *Lithos*, *178*, 96–127. https://doi.org/10.1016/j.lithos.2013.05.019

Dewey, J. F., & Bird, J. M. (1970). Mountain belts and the new global tectonics. *Journal of Geophysical Research (1896–1977)*, *75*(14), 2625–2647. https://doi.org/10.1029/JB075i014p02625

Donoso-Tapia, D., Flores, K. E., Martin, C., Gazel, E., & Marsh, J. (2024). Exhumed serpentinites and their tectonic significance in non-collisional orogens [Dataset]. https://doi.org/10.26022/IEDA/112939

Donoso-Tapia, D., Herviou, C., & Flores, K. E. (2022). Tectonic significance of exhumed subduction-related metamorphic rocks in Cordilleran Orogens. In *AGU fall meeting, Chicago, IL*.

Duhart, P., & Adriasola, A. C. (2008). New time-constraints on provenance, metamorphism and exhumation of the Bahía Mansa Metamorphic Complex on the Main Chiloé Island, south-central Chile. *Andean Geology*, *35*(1), 79–104. https://doi.org/10.5027/andgeov35n1-a04

Duhart, P., McDonough, M., Muñoz, J., Martin, M., & Villeneuve, M. (2001). El Complejo Metamórfico Bahía Mansa en la cordillera de la Costa del centro-sur de Chile (39° 30′-42° 00'S): Geocronología K-Ar, 40Ar/39Ar y U-Pb e implicancias en la evolución del margen sur-occidental de Gondwana. *Revista Geológica de Chile*, *28*(2), 179–208. https://doi.org/10.4067/s0716-02082001000200003

Duretz, T., Gerya, T. V., Kaus, B. J. P., & Andersen, T. B. (2012). Thermomechanical modeling of slab eduction. *Journal of Geophysical Research*, *117*(B8). https://doi.org/10.1029/2012JB009137

Duretz, T., Gerya, T. V., & May, D. A. (2011). Numerical modelling of spontaneous slab breakoff and subsequent topographic response. *Tectonophysics*, *502*(1), 244–256. https://doi.org/10.1016/j.tecto.2010.05.024

Eguez, A., Gaona, M., & Albán, A. (2017). Mapa Geológico de la República del Ecuador 2017.

Evans, B. W. (2004). The serpentinite multisystem revisited: Chrysotile is metastable. *International Geology Review*, *46*(6), 479–506. https://doi.org/10.2747/0020-6814.46.6.479

Evans, B. W., Hattori, K., & Baronnet, A. (2013). Serpentinite: What, why, where? *Elements*, *9*(2), 99–106. https://doi.org/10.2113/gselements.9.2.99

Evans, K. A., & Frost, B. R. (2021). Deserpentinization in subduction zones as a source of oxidation in arcs: A reality check. *Journal of Petrology*, *62*(3), egab016. https://doi.org/10.1093/petrology/egab016

Evans, K. A., Powell, R., & Frost, B. R. (2013). Using equilibrium thermodynamics in the study of metasomatic alteration, illustrated by an application to serpentinites. *Lithos*, *168–169*, 67–84. https://doi.org/10.1016/j.lithos.2013.01.016

Faccenna, C., Becker, T. W., Holt, A. F., & Brun, J. P. (2021). Mountain building, mantle convection, and supercontinents: Holmes (1931) revisited. *Earth and Planetary Science Letters*, *564*, 116905. https://doi.org/10.1016/j.epsl.2021.116905

Faccenna, C., Oncken, O., Holt, A. F., & Becker, T. W. (2017). Initiation of the Andean orogeny by lower mantle subduction. *Earth and Planetary Science Letters*, *463*, 189–201. https://doi.org/10.1016/j.epsl.2017.01.041

Feininger, T., & Silberman, M. L. (1982). *K-Ar geochronology of basement rocks on the northern flank of the Huancabama deflection, Ecuador*. [Open-File Report, Issue, Report] (82-206). U. S. G. Survey. Retrieved from http://pubs.er.usgs.gov/publication/ofr82206

Flores, K. E., Marsh, J., Strauss, B., & Estrada, N. (2019). Metamorphic evolution and exhumation of high-pressure assemblages of the Cordillera Real (Ecuador). In *AGU fall meeting, San Francisco, CA*.

Flores, K. E., Martens, U. C., Harlow, G. E., Brueckner, H. K., & Pearson, N. J. (2013). Jadeitite formed during subduction: In situ zircon geochronology constraints from two different tectonic events within the Guatemala Suture Zone. *Earth and Planetary Science Letters*, *371–372*, 67–81. https://doi.org/10.1016/j.epsl.2013.04.015

Flores, K. E., Skora, S., Martin, C., Harlow, G. E., Rodríguez, D., & Baumgartner, P. O. (2015). Metamorphic history of riebeckite- and aegirine-augite-bearing high-pressure–low-temperature blocks within the Siuna Serpentinite Mélange, northeastern Nicaragua. *International Geology Review*, *57*(5–8), 943–977. https://doi.org/10.1080/00206814.2015.1027747

Gabriele, P. (2002). *HP terranes exhumation in an active margin setting: Geology, petrology and geochemistry of the Raspas Complex in SW Ecuador*. Université de Lausanne.

Gamal El Dien, H., Arai, S., Doucet, L.-S., Li, Z.-X., Kil, Y., Fougerouse, D., et al. (2019). Cr-spinel records metasomatism not petrogenesis of mantle rocks. *Nature Communications*, *10*(1), 5103. https://doi.org/10.1038/s41467-019-13117-1

Garcia-Casco, A., Restrepo, J. J., Correa–Martínez, A. M., Blanco-Quintero, I. F., Proenza, J. A., Weber, M., & Butjosa, L. (2020). The petrologic nature of the "Medellín Dunite" revisited: An algebraic approach and proposal of a new definition of the geological body. In J. Gómez & A. O. Pinilla–Pachon (Eds.), *The geology of Colombia, Volume 2 Mesozoic* (Vol. 36, pp. 45–75). Servicio Geológico Colombiano, Publicaciones Geológicas Especiales. https://doi.org/10.32685/pub.esp.36.2019.02

García-Ramírez, C. A., Rios-Reyes, O. M., Castellanos-Alarcon, O. M., & Mantilla-Figueroa, L. C. (2017). Petrology, geochemistry and geochronology of the arquía complex's metabasites at the Pijao-Génova sector, Central Cordillera, Colombian Andes. *Revista Boletín de Geología*, *39*(1), 105–126. https://doi.org/10.18273/revbol.v39n1-2017005

George, S. W. M., Horton, B. K., Vallejo, C., Jackson, L. J., & Gutierrez, E. G. (2021). Did accretion of the Caribbean oceanic plateau drive rapid crustal thickening in the northern Andes? *Geology*, *49*(8), 936–940. https://doi.org/10.1130/G48509.1

Gilio, M., Scambelluri, M., Agostini, S., Godard, M., Peters, D., & Pettke, T. (2019). Petrology and geochemistry of serpentinites associated with the ultra-high pressure Lago di Cignana Unit (Italian Western Alps). *Journal of Petrology*, *60*(6), 1229–1262. https://doi.org/10.1093/petrology/egz030

Glodny, J., Echtler, H., Collao, S., Ardiles, M., Burón, P., & Figueroa, O. (2008). Differential Late Paleozoic active margin evolution in South-Central Chile (37°S–40°S) – The Lanalhue Fault Zone. *Journal of South American Earth Sciences*, *26*(4), 397–411. https://doi.org/10.1016/j.jsames.2008.06.001

Glodny, J., Lohrmann, J., Echtler, H., Gräfe, K., Seifert, W., Collao, S., & Figueroa, O. (2005). Internal dynamics of a paleoaccretionary wedge: Insights from combined isotope tectonochronology and sandbox modelling of the South-Central Chilean forearc. *Earth and Planetary Science Letters*, *231*(1), 23–39. https://doi.org/10.1016/j.epsl.2004.12.014

González-Jiménez, J. M., Kerestedjian, T., Proenza-Fernández, J. A., & Gervilla-Linares, F. (2009). Metamorphism on chromite ores from the Dobromirtsi ultramafic massif, Rhodope Mountains (SE Bulgaria). *Geológica Acta*, *7*(4), 413–429.

González-Jiménez, J. M., Plissart, G., Garrido, L. N., Padrón-Navarta, J. A., Aiglsperger, T., Romero, R., et al. (2017). Titanian clinohumite and chondrodite in antigorite serpentinites from Central Chile: Evidence for deep and cold subduction. *European Journal of Mineralogy*, *29*(6), 959–970. https://doi.org/10.1127/ejm/2017/0029-2668

Green, E. C. R., White, R. W., Diener, J. F. A., Powell, R., Holland, T. J. B., & Palin, R. M. (2016). Activity–composition relations for the calculation of partial melting equilibria in metabasic rocks. *Journal of Metamorphic Geology*, *34*(9), 845–869. https://doi.org/10.1111/jmg.12211

Groppo, C., Rinaudo, C., Cairo, S., Gastaldi, D., & Compagnoni, R. (2006). Micro-Raman spectroscopy for a quick and reliable identification of serpentine minerals from ultramafics. *European Journal of Mineralogy*, *18*(3), 319–329. https://doi.org/10.1127/0935-1221/2006/0018-0319

Grunow, A. M., Dalziel, I. W. D., Harrison, T. M., & Heizler, M. T. (1992). Structural geology and geochronology of subduction complexes along the margin of Gondwanaland: New data from the Antarctic Peninsula and southernmost Andes. *GSA Bulletin*, *104*(11), 1497–1514. https://doi.org/10.1130/0016-7606(1992)104<1497:sgagos>2.3.co;2

Guillot, S., Hattori, K., Agard, P., Schwartz, S., & Vidal, O. (2009). Exhumation processes in oceanic and continental subduction contexts: A review. In *Subduction zone geodynamics*.

Halama, R., Savov, I. P., Garbe-Schönberg, D., Schenk, V., & Toulkeridis, T. (2013). Vesuvianite in high-pressure-metamorphosed oceanic lithosphere (Raspas Complex, Ecuador) and its role for transport of water and trace elements in subduction zones. *European Journal of Mineralogy*, *25*(2), 193–219. https://doi.org/10.1127/0935-1221/2013/0025-2281

Halpern, M. (1973). Regional geochronology of Chile south of 50 latitude. *Geological Society of America Bulletin*, *84*(7), 2407–2422. https://doi.org/10.1130/0016-7606(1973)84<2407:rgocso>2.0.co;2

Hanghøj, K., Kelemen, P. B., Hassler, D., & Godard, M. (2010). Composition and genesis of depleted mantle peridotites from the Wadi Tayin Massif, Oman Ophiolite; Major and trace element geochemistry, and Os isotope and PGE Systematics. *Journal of Petrology*, *51*(1–2), 201–227. https://doi.org/10.1093/petrology/egp077

Hanson, B. A. (2014). ChemoSpec: An R package for chemometric analysis of spectroscopic data and chromatograms. (Package Version 2.0-2).

Harvey, J., Garrido, C. J., Savov, I., Agostini, S., Padrón-Navarta, J. A., Marchesi, C., et al. (2014). ^{11}B-rich fluids in subduction zones: The role of antigorite dehydration in subducting slabs and boron isotope heterogeneity in the mantle. *Chemical Geology*, *376*, 20–30. https://doi.org/10.1016/j.chemgeo.2014.03.015

Hässig, M., Rolland, Y., Duretz, T., & Sosson, M. (2016). Obduction triggered by regional heating during plate reorganization. *Terra Nova*, *28*(1), 76–82. https://doi.org/10.1111/ter.12193

Hawthorne, F. C., Oberti, R., Harlow, G. E., Maresch, W. V., Martin, R. F., Schumacher, J. C., & Welch, M. D. (2012). Nomenclature of the amphibole supergroup. *American Mineralogist*, *97*(11–12), 2031–2048. https://doi.org/10.2138/am.2012.4276

Herms, P., John, T., Bakker, R. J., & Schenk, V. (2012). Evidence for channelized external fluid flow and element transfer in subducting slabs (Raspas Complex, Ecuador). *Chemical Geology*, *310–311*, 79–96. https://doi.org/10.1016/j.chemgeo.2012.03.023

Hervé, F. (1988). Late Paleozoic subduction and accretion in Southern Chile. *International Union of Geological Sciences*, *11*(3), 183–188. https://doi.org/10.18814/epiiugs/1988/v11i3/005

Hervé, F., Nelson, E., Kawashita, K., & Suárez, M. (1981). New isotopic ages and the timing of orogenic events in the Cordillera Darwin, southernmost Chilean Andes. *Earth and Planetary Science Letters*, *55*(2), 257–265. https://doi.org/10.1016/0012-821X(81)90105-9

Höfer, C., Kraus, S., Miller, H., Alfaro, G., & Barra, F. (2001). Chromite-bearing serpentinite bodies within an arc–backarc metamorphic complex near La Cabaña, south Chilean Coastal Cordillera. *Journal of South American Earth Sciences*, *14*(1), 113–126. https://doi.org/10.1016/S0895-9811(01)00011-6

Holland, T. J. B., & Powell, R. (1998). An internally consistent thermodynamic data set for phases of petrological interest. *Journal of Metamorphic Geology*, *16*(3), 309–343. https://doi.org/10.1111/j.1525-1314.1998.00140.x

Holland, T. J. B., & Powell, R. (2011). An improved and extended internally consistent thermodynamic dataset for phases of petrological interest, involving a new equation of state for solids. *Journal of Metamorphic Geology*, *29*(3), 333–383. https://doi.org/10.1111/j.1525-1314.2010.00923.x

Hyppolito, T., Angiboust, S., Juliani, C., Glodny, J., Garcia-Casco, A., Calderón, M., & Chopin, C. (2016). Eclogite-amphibolite- and blueschist-facies rocks from Diego de Almagro Island (Patagonia): Episodic accretion and thermal evolution of the Chilean subduction interface during the Cretaceous. *Lithos*, *264*, 422–440. https://doi.org/10.1016/j.lithos.2016.09.001

Hyppolito, T., García-Casco, A., Juliani, C., Meira, V. T., & Hall, C. (2014). Late Paleozoic onset of subduction and exhumation at the western margin of Gondwana (Chilenia Terrane): Counterclockwise P–T paths and timing of metamorphism of deep-seated garnet–mica schist and amphibolite of Punta Sirena, Coastal Accretionary Complex, central Chile (34° S). *Lithos*, *206–207*, 409–434. https://doi.org/10.1016/j.lithos.2014.07.023

Ibañez-Mejia, M., Restrepo, J., & Garcia-Casco, A. (2020). Tectonic juxtaposition of Triassic and Cretaceous meta-(ultra)mafic complexes in the Central Cordillera of Colombia (Medellin area) revealed by zircon U-Pb geochronology and Lu-Hf isotopes. In A. Bartorelli, W. Teixeira, & B. B. Brito Neves (Eds.), *Geocronologia e Evolução Tectônica do Continente Sul-Americano: A contribuição de Umberto Giuseppe Cordani* (Vol. 1, pp. 418–443). Solaris.

Jennings, E. S., & Holland, T. J. B. (2015). A simple thermodynamic model for melting of peridotite in the system NCFMASOCr. *Journal of Petrology*, *56*(5), 869–892. https://doi.org/10.1093/petrology/egv020

John, T., Scherer, E., Schenk, V., Herms, P., Halama, R., & Garbe-Schönberg, D. (2010). Subducted seamounts in an eclogite-facies ophiolite sequence: The Andean Raspas Complex, SW Ecuador. *Contributions to Mineralogy and Petrology*, *159*(2), 265–284. https://doi.org/10.1007/s00410-009-0427-0

Kato, T. T., & Godoy, E. (1995). Petrogenesis and tectonic significance of Late Paleozoic coarse-crystalline blueschist and amphibolite boulders in the coastal range of Chile. *International Geology Review*, *37*(11), 992–1006. https://doi.org/10.1080/00206819509465437

Kato, T. T., Sharp, W. D., & Godoy, E. (2008). Inception of a Devonian subduction zone along the southwestern Gondwana margin: ^{40}Ar–^{39}Ar dating of eclogite–amphibolite assemblages in blueschist boulders from the Coastal Range of Chile (41°S). *Canadian Journal of Earth Sciences*, *45*(3), 337–351. https://doi.org/10.1139/E08-006

Klepeis, K., Betka, P., Clarke, G., Fanning, M., Hervé, F., Rojas, L., et al. (2010). Continental underthrusting and obduction during the Cretaceous closure of the Rocas Verdes rift basin, Cordillera Darwin, Patagonian Andes. *Tectonics*, *29*(3), TC3014. https://doi.org/10.1029/2009TC002610

Kohn, M. J., Spear, F. S., Harrison, T. M., & Dalziel, I. W. D. (1995). $^{40}Ar/^{39}Ar$ geochronology and P-T-t paths from the Cordillera Darwin metamorphic complex, Tierra del Fuego, Chile. *Journal of Metamorphic Geology*, *13*(2), 251–270. https://doi.org/10.1111/j.1525-1314.1995.tb00217.x

Lafay, R., Deschamps, F., Schwartz, S., Guillot, S., Godard, M., Debret, B., & Nicollet, C. (2013). High-pressure serpentinites, a trap-and-release system controlled by metamorphic conditions: Example from the Piedmont zone of the western Alps. *Chemical Geology*, *343*, 38–54. https://doi.org/10.1016/j.chemgeo.2013.02.008

Lécuyer, C., Grandjean, P., Reynard, B., Albarède, F., & Telouk, P. (2002). $^{11}B/^{10}B$ analysis of geological materials by ICP–MS Plasma 54: Application to the boron fractionation between brachiopod calcite and seawater. *Chemical Geology*, *186*(1), 45–55. https://doi.org/10.1016/S0009-2541(01)00425-9

Litherland, M., Aspden, J. A., & Jemielita, R. A. (1994). The metamorphic belts of Ecuador.

Maloney, K. T., Clarke, G. L., Klepeis, K. A., Fanning, C. M., & Wang, W. (2011). Crustal growth during back-arc closure: Cretaceous exhumation history of Cordillera Darwin, southern Patagonia. *Journal of Metamorphic Geology*, *29*(6), 649–672. https://doi.org/10.1111/j.1525-1314.2011.00934.x

Marschall, H. R., Altherr, R., & Rüpke, L. (2007). Squeezing out the slab — Modelling the release of Li, Be and B during progressive high-pressure metamorphism. *Chemical Geology*, *239*(3), 323–335. https://doi.org/10.1016/j.chemgeo.2006.08.008

Martin, C., Flores, K. E., & Harlow, G. E. (2016). Boron isotopic discrimination for subduction-related serpentinites. *Geology*, *44*(11), 899–902. https://doi.org/10.1130/g38102.1

Martin, C., Flores, K. E., Harlow, G. E., Angiboust, S., Hodel, F., & Guice, G. L. (2023). The B isotopic signature of serpentine from obducted ophiolites: Mixing of fluids and tectonic implications. *Lithos*, *456–457*, 107275. https://doi.org/10.1016/j.lithos.2023.107275

Martin, C., Flores, K. E., Vitale-Brovarone, A., Angiboust, S., & Harlow, G. E. (2020). Deep mantle serpentinization in subduction zones: Insight from in situ B isotopes in slab and mantle wedge serpentinites. *Chemical Geology*, *545*, 119637. https://doi.org/10.1016/j.chemgeo.2020.119637

Martin, C., Ponzevera, E., & Harlow, G. (2015). In situ lithium and boron isotope determinations in mica, pyroxene, and serpentine by LA-MC-ICP-MS. *Chemical Geology*, *412*, 107–116. https://doi.org/10.1016/j.chemgeo.2015.07.022

Martínez, J. C., Dristas, J. A., & Massonne, H.-J. (2012). Palaeozoic accretion of the microcontinent Chilenia, North Patagonian Andes: High-pressure metamorphism and subsequent thermal relaxation. *International Geology Review*, *54*(4), 472–490. https://doi.org/10.1080/00206814.2011.569411

Massonne, H.-J., & Toulkeridis, T. (2012). Widespread relics of high-pressure metamorphism confirm major terrane accretion in Ecuador: A new example from the Northern Andes. *International Geology Review*, *54*(1), 67–80. https://doi.org/10.1080/00206814.2010.498907

McDonough, W. F., & Sun, S. S. (1995). The composition of the Earth. *Chemical Geology*, *120*(3), 223–253. https://doi.org/10.1016/0009-2541(94)00140-4

Mellini, M., Trommsdorff, V., & Compagnoni, R. (1987). Antigorite polysomatism: Behaviour during progressive metamorphism. *Contributions to Mineralogy and Petrology*, *97*(2), 147–155. https://doi.org/10.1007/BF00371235

Morimoto, N., Fabries, J., Ferguson, A. K., Ginzburg, I. V., Ross, M., Seifert, F. A., et al. (1988). Nomenclature of pyroxenes. *American Mineralogist*, *73*(9–10), 1123–1133. Retrieved from http://ammin.geoscienceworld.org/content/73/9-10/1123.short

Niu, Y. (2004). Bulk-rock major and trace element compositions of abyssal peridotites: Implications for mantle melting, melt extraction and post-melting processes beneath mid-ocean ridges. *Journal of Petrology*, *45*(12), 2423–2458. https://doi.org/10.1093/petrology/egh068

Padrón-Navarta, J. A., Hermann, J., Garrido, C. J., López Sánchez-Vizcaíno, V., & Gómez-Pugnaire, M. T. (2010). An experimental investigation of antigorite dehydration in natural silica-enriched serpentinite. *Contributions to Mineralogy and Petrology*, *159*(1), 25–42. https://doi.org/10.1007/s00410-009-0414-5

Padrón-Navarta, J. A., López Sánchez-Vizcaíno, V., Garrido, C. J., & Gómez-Pugnaire, M. T. (2011). Metamorphic record of high-pressure dehydration of antigorite serpentinite to chlorite harzburgite in a subduction setting (Cerro del Almirez, Nevado–Filábride Complex, Southern Spain). *Journal of Petrology*, *52*(10), 2047–2078. https://doi.org/10.1093/petrology/egr039

Padrón-Navarta, J. A., Sánchez-Vizcaíno, V. L., Hermann, J., Connolly, J. A. D., Garrido, C. J., Gómez-Pugnaire, M. T., & Marchesi, C. (2013). Tschermak's substitution in antigorite and consequences for phase relations and water liberation in high-grade serpentinites. *Lithos*, *178*, 186–196. https://doi.org/10.1016/j.lithos.2013.02.001

Pagé, L., Hattori, K., & Guillot, S. (2018). Mantle wedge serpentinites: A transient reservoir of halogens, boron, and nitrogen for the deeper mantle. *Geology*, *46*(10), 883–886. https://doi.org/10.1130/G45204.1

Parkinson, I. J., & Pearce, J. A. (1998). Peridotites from the Izu–Bonin–Mariana Forearc (ODP Leg 125): Evidence for mantle melting and melt–mantle interaction in a supra-subduction zone setting. *Journal of Petrology*, *39*(9), 1577–1618. https://doi.org/10.1093/petroj/39.9.1577

Paton, C., Hellstrom, J., Paul, B., Woodhead, J., & Hergt, J. (2011). Iolite: Freeware for the visualisation and processing of mass spectrometric data. *Journal of Analytical Atomic Spectrometry*, *26*(12), 2508–2518. https://doi.org/10.1039/C1JA10172B

Peters, D., Bretscher, A., John, T., Scambelluri, M., & Pettke, T. (2017). Fluid-mobile elements in serpentinites: Constraints on serpentinisation environments and element cycling in subduction zones. *Chemical Geology*, *466*, 654–666. https://doi.org/10.1016/j.chemgeo.2017.07.017

Pettke, T., & Bretscher, A. (2022). Fluid-mediated element cycling in subducted oceanic lithosphere: The orogenic serpentinite perspective. *Earth-Science Reviews*, *225*, 103896. https://doi.org/10.1016/j.earscirev.2021.103896

Plissart, G., González-Jiménez, J. M., Garrido, L. N. F., Colás, V., Berger, J., Monnier, C., et al. (2019). Tectono-metamorphic evolution of subduction channel serpentinites from South-Central Chile. *Lithos*, *336–337*, 221–241. https://doi.org/10.1016/j.lithos.2019.03.023

Powell, R., & Holland, T. (1999). Relating formulations of the thermodynamics of mineral solid solutions; activity modeling of pyroxenes, amphiboles, and micas. *American Mineralogist*, *84*(1–2), 1–14. https://doi.org/10.2138/am-1999-1-201

Pratt, W. T., Duque, P., & Ponce, M. (2005). An autochthonous geological model for the eastern Andes of Ecuador. *Tectonophysics*, *399*(1), 251–278. https://doi.org/10.1016/j.tecto.2004.12.025

Prigent, C., Guillot, S., Agard, P., Lemarchand, D., Soret, M., & Ulrich, M. (2018). Transfer of subduction fluids into the deforming mantle wedge during nascent subduction: Evidence from trace elements and boron isotopes (Semail ophiolite, Oman). *Earth and Planetary Science Letters*, *484*, 213–228. https://doi.org/10.1016/j.epsl.2017.12.008

Raia, N. H., Whitney, D. L., Teyssier, C., & Lesimple, S. (2022). Serpentinites of different tectonic origin in an exhumed subduction complex (New Caledonia, SW Pacific). *Geochemistry, Geophysics, Geosystems*, *23*(8), e2022GC010395. https://doi.org/10.1029/2022GC010395

Ramos, V. A. (1988). Late Proterozoic-Early Paleozoic of South America - A collisional history. *International Union of Geological Sciences*, *11*(3), 168–174. https://doi.org/10.18814/epiiugs/1988/v11i3/003

Ramos, V. A. (2008). The basement of the Central Andes: The arequipa and related terranes. *Annual Review of Earth and Planetary Sciences*, *36*(1), 289–324. https://doi.org/10.1146/annurev.earth.36.031207.124304

Ramos, V. A., Dallmeyer, R. D., & Vujovich, G. (1998). Time constraints on the Early Palaeozoic docking of the Precordillera, central Argentina. *Geological Society, London, Special Publications*, *142*(1), 143–158. https://doi.org/10.1144/GSL.SP.1998.142.01.08

Riel, N., Guillot, S., Jaillard, E., Martelat, J. E., Paquette, J. L., Schwartz, S., et al. (2013). Metamorphic and geochronogical study of the Triassic El Oro metamorphic complex, Ecuador: Implications for high-temperature metamorphism in a forearc zone. *Lithos*, *156–159*, 41–68. https://doi.org/10.1016/j.lithos.2012.10.005

Rojo, D., Calderón, M., Hervé, F., Díaz, J., Quezada, P., Suárez, R., et al. (2021). Petrology and tectonic evolution of late Paleozoic mafic-ultramafic sequences and the Leones Pluton of the Eastern Andean Metamorphic Complex (46-47°S), southern Chile. *Journal of South American Earth Sciences*, *108*, 103198. https://doi.org/10.1016/j.jsames.2021.103198

Romero, R., González-Jiménez, J. M., Barra, F., Leisen, M., Garrido, L. N., Talavera, C., et al. (2018). Timing the tectonic mingling of ultramafic rocks and metasediments in the southern section of the coastal accretionary complex of central Chile. *International Geology Review*, *60*(16), 2031–2045. https://doi.org/10.1080/00206814.2017.1402377

Romeuf, N., Aguirre, L., Soler, P., Feraud, G., Jaillard, E., & Ruffet, G. (1995). Middle Jurassic volcanism in the northern and central Andes. *Andean Geology*, *22*(2), 245–259.

Sadekov, A., Lloyd, N. S., Misra, S., Trotter, J., D'Olivo, J., & McCulloch, M. (2019). Accurate and precise microscale measurements of boron isotope ratios in calcium carbonates using laser ablation multicollector-ICPMS. *Journal of Analytical Atomic Spectrometry*, *34*(3), 550–560. https://doi.org/10.1039/C8JA00444G

Sanhueza, J., Yáñez, G., Barra, F., Maringue, J., Figueroa, R., & Sáez, E. (2022). Rheological, petrophysical and geometrical constraints of a subduction channel from a numerical model perspective: Insights from La Cabaña Paleozoic peridotites, Coastal Cordillera of south-central Chile. *Journal of South American Earth Sciences*, *114*, 103706. https://doi.org/10.1016/j.jsames.2021.103706

Saumur, B. M., & Hattori, K. (2013). Zoned Cr-spinel and ferritchromite alteration in forearc mantle serpentinites of the Rio San Juan Complex, Dominican Republic. *Mineralogical Magazine*, *77*(1), 117–136. https://doi.org/10.1180/minmag.2013.077.1.11

Schwartz, S., Lardeaux, J.-M., Guillot, S., & Tricart, P. (2000). Diversité du métamorphisme éclogitique dans le massif ophiolitique du Monviso (Alpes occidentales, Italie). *Geodinamica Acta*, *13*(2–3), 169–188. https://doi.org/10.1080/09853111.2000.11105371

Shen, T., Hermann, J., Zhang, L., Lü, Z., Padrón-Navarta, J. A., Xia, B., & Bader, T. (2015). UHP Metamorphism documented in Ti-chondrodite- and Ti-clinohumite-bearing serpentinized ultramafic rocks from Chinese Southwestern Tianshan. *Journal of Petrology*, *56*(7), 1425–1458. https://doi.org/10.1093/petrology/egv042

Sisson, V. B., Cardoso, R. K., Harris, C. C., Huang, S., & Unger, L. M. (2005). Exhumation history of two high-pressure belts, northern Venezuela, based on fluid inclusions in quartz and calcite veins. *Geological Society of America Special Papers*, *394*, 157–171. https://doi.org/10.1130/0-8137-2394-9.157

Sisson, V. B., Ertan, I. E., & Lallemant, H. G. A. (1997). High-pressure (~2000 MPa) kyanite- and glaucophane-bearing pelitic schist and eclogite from Cordillera de la Costa Belt, Venezuela. *Journal of Petrology*, *38*(1), 65–83. https://doi.org/10.1093/petroj/38.1.65

Smith, C. A., Sisson, V. B., Avé Lallemant, H. G., & Copeland, P. (1999). Two contrasting pressure-temperature-time paths in the Villa de Cura blueschist belt, Venezuela: Possible evidence for Late Cretaceous initiation of subduction in the Caribbean. *GSA Bulletin*, *111*(6), 831–848. https://doi.org/10.1130/0016-7606(1999)111<0831:TCPTTP>2.3.CO;2

Spikings, R., Cochrane, R., Villagomez, D., Van der Lelij, R., Vallejo, C., Winkler, W., & Beate, B. (2015). The geological history of north-western South America: From Pangaea to the early collision of the Caribbean Large Igneous Province (290–75Ma). *Gondwana Research*, *27*(1), 95–139. https://doi.org/10.1016/j.gr.2014.06.004

Spikings, R., Paul, A., Vallejo, C., & Reyes, P. (2021). Constraints on the ages of the crystalline basement and Palaeozoic cover exposed in the Cordillera Real, Ecuador: $^{40}Ar/^{39}Ar$ analyses and detrital zircon U/Pb geochronology. *Gondwana Research*, *90*, 77–101. https://doi.org/10.1016/j.gr.2020.10.009

Spikings, R. A., Winkler, W., Seward, D., & Handler, R. (2001). Along-strike variations in the thermal and tectonic response of the continental Ecuadorian Andes to the collision with heterogeneous oceanic crust. *Earth and Planetary Science Letters*, *186*(1), 57–73. https://doi.org/10.1016/S0012-821X(01)00225-4

Stöckhert, B., Maresch, W. V., Brix, M., Kaiser, C., Toetz, A., Kluge, R., & Krückhans-Lueder, G. (1995). Crustal history of Margarita Island (Venezuela) in detail: Constraint on the Caribbean plate-tectonic scenario. *Geology*, *23*(9), 787–790. https://doi.org/10.1130/0091-7613(1995)023<0787:chomiv>2.3.co;2

Suhr, N., Rojas-Agramonte, Y., Chew, D. M., Pinto, A. J., Villagómez-Díaz, D., Toulkeridis, T., & Mertz-Kraus, R. (2019). Detrital-zircon geochronology and provenance of the El Oro Metamorphic Complex, Ecuador: Geodynamic implications for the evolution of the western Gondwana margin. *Journal of South American Earth Sciences*, *90*, 520–539. https://doi.org/10.1016/j.jsames.2018.12.010

Tamblyn, R., Zack, T., Schmitt, A. K., Hand, M., Kelsey, D., Morrissey, L., et al. (2019). Blueschist from the Mariana forearc records long-lived residence of material in the subduction channel. *Earth and Planetary Science Letters*, *519*, 171–181. https://doi.org/10.1016/j.epsl.2019.05.013

Toussaint, J. F., & Restrepo, J. J. (1978). Edad cretácea de una anfibolita granatífera de Pijao-Quindío. *Boletín de Ciencias de la Tierra*(5–6), 77–78. Retrieved from https://revistas.unal.edu.co/index.php/rbct/article/view/94418

van Staal, C. R., Vujovich, G. I., Currie, K. L., & Naipauer, M. (2011). An Alpine-style Ordovician collision complex in the Sierra de Pie de Palo, Argentina: Record of subduction of Cuyania beneath the Famatina arc. *Journal of Structural Geology*, *33*(3), 343–361. https://doi.org/10.1016/j.jsg.2010.10.011

Viete, D. R., Kylander-Clark, A. R. C., & Hacker, B. R. (2015). Single-shot laser ablation split stream (SS-LASS) petrochronology deciphers multiple, short-duration metamorphic events. *Chemical Geology*, *415*, 70–86. https://doi.org/10.1016/j.chemgeo.2015.09.013

Villagómez, D., Spikings, R., Magna, T., Kammer, A., Winkler, W., & Beltrán-Triviño, A. (2011). Geochronology, geochemistry and tectonic evolution of the Western and Central Cordilleras of Colombia. *Lithos*, *125*(3–4), 875–896. https://doi.org/10.1016/j.lithos.2011.05.003

Villares, F., Garcia-Casco, A., Blanco-Quintero, I. F., Montes, C., Reyes, P. S., & Cardona, A. (2021). The Peltetec ophiolitic belt (Ecuador): A window to the tectonic evolution of the Triassic margin of western Gondwana. *International Geology Review*, *63*(18), 2232–2256. https://doi.org/10.1080/00206814.2020.1830313

Vils, F., Tonarini, S., Kalt, A., & Seitz, H.-M. (2009). Boron, lithium and strontium isotopes as tracers of seawater–serpentinite interaction at Mid-Atlantic ridge, ODP Leg 209. *Earth and Planetary Science Letters*, *286*(3), 414–425. https://doi.org/10.1016/j.epsl.2009.07.005

Vujovich, G. I., van Staal, C. R., & Davis, W. (2004). Age constraints on the tectonic evolution and provenance of the Pie de Palo Complex, Cuyania composite terrane, and the Famatinian Orogeny in the Sierra de Pie de Palo, San Juan, Argentina. *Gondwana Research*, *7*(4), 1041–1056. https://doi.org/10.1016/S1342-937X(05)71083-2

Walters, J. B. (2022). MinPlot: A mineral formula recalculation and plotting program for electron probe microanalysis. *Mineralogia*, *53*(1), 51–66. https://doi.org/10.2478/mipo-2022-0005

Warren, J. M. (2016). Global variations in abyssal peridotite compositions. *Lithos*, *248–251*, 193–219. https://doi.org/10.1016/j.lithos.2015.12.023

Weber, M., Cardona, A., Valencia, V., Altenberger, U., López Martínez, M., Tobón, M., et al. (2011). Geochemistry and Geochronology of the Guajira Eclogites, northern Colombia: Evidence of a metamorphosed primitive Cretaceous Caribbean Island-arc. *Geológica Acta*, *9*(3–4), 425–443.

Weber, M., Cardona, A., Wilson, R., Gómez, J., & Zapata, G. (2007). Quimica Mineral de las rocas de altra presion - Facies eclogita, de La peninsula de la Guajira, Colombia. *Boletín de Geología*, *29*(1), 31–39. Retrieved from https://revistas.uis.edu.co/index.php/revistaboletindegeologia/article/view/847

Whitney, D. L., & Evans, B. W. (2010). Abbreviations for names of rock-forming minerals. *American Mineralogist*, *95*(1), 185–187. https://doi.org/10.2138/am.2010.3371

Willner, A. P. (2005). Pressure–temperature evolution of a Late Palaeozoic paired metamorphic belt in North–Central Chile (34°–35°30′S). *Journal of Petrology*, *46*(9), 1805–1833. https://doi.org/10.1093/petrology/egi035

Willner, A. P., Gerdes, A., Massonne, H.-J., Schmidt, A., Sudo, M., Thomson, S. N., & Vujovich, G. (2011). The geodynamics of collision of a microplate (Chilenia) in Devonian times deduced by the pressure–temperature–time evolution within part of a collisional belt (Guarguaraz Complex, W-Argentina). *Contributions to Mineralogy and Petrology*, *162*(2), 303–327. https://doi.org/10.1007/s00410-010-0598-8

Willner, A. P., Glodny, J., Gerya, T. V., Godoy, E., & Massonne, H. J. (2004). A counterclockwise PTt path of high-pressure/low-temperature rocks from the Coastal Cordillera accretionary complex of south-central Chile: Constraints for the earliest stage of subduction mass flow. *Lithos*, *75*(3), 283–310. https://doi.org/10.1016/j.lithos.2004.03.002

Willner, A. P., Massonne, H. J., Gerdes, A., Hervé, F., Sudo, M., & Thomson, S. (2009). The contrasting evolution of collisional and coastal accretionary systems between the latitudes 30 S and 35 S: Evidence for the existence of a Chilenia microplate. In *XII Congreso Geológico Chileno, Santiago*.

Willner, A. P., Massonne, H.-J., Ring, U. W. E., Sudo, M., & Thomson, S. N. (2012). P–T evolution and timing of a late Palaeozoic fore-arc system and its heterogeneous Mesozoic overprint in north-central Chile (latitudes 31–32°S). *Geological Magazine*, *149*(2), 177–207. https://doi.org/10.1017/S0016756811000641

Willner, A. P., Tassinari, C. C. G., Rodrigues, J. F., Acosta, J., Castroviejo, R., & Rivera, M. (2014). Contrasting Ordovician high- and low-pressure metamorphism related to a microcontinent-arc collision in the Eastern Cordillera of Perú (Tarma province). *Journal of South American Earth Sciences*, *54*, 71–81. https://doi.org/10.1016/j.jsames.2014.05.001

Willner, A. P., Thomson, S. N., KrÖNer, A., Wartho, J.-A., Wijbrans, J. R., & HervÉ, F. (2005). Time markers for the evolution and exhumation history of a Late Palaeozoic paired metamorphic belt in North–Central Chile (34°–35°30′S). *Journal of Petrology*, *46*(9), 1835–1858. https://doi.org/10.1093/petrology/egi036

Wu, K., Zhang, L., Yuan, H., Sun, W., Deng, J., Zartman, R. E., et al. (2021). Boron, arsenic and antimony recycling in subduction zones: New insights from interactions between forearc serpentinites and CO_2-rich fluids at the slab-mantle interface. *Geochimica et Cosmochimica Acta*, *298*, 21–42. https://doi.org/10.1016/j.gca.2021.01.039

Wunder, B., Meixner, A., Romer, R. L., Wirth, R., & Heinrich, W. (2005). The geochemical cycle of boron: Constraints from boron isotope partitioning experiments between mica and fluid. *Lithos*, *84*(3), 206–216. https://doi.org/10.1016/j.lithos.2005.02.003

Yamada, C., Tsujimori, T., Chang, Q., & Kimura, J.-I. (2019). Boron isotope variations of Franciscan serpentinites, Northern California. *Lithos*, *334–335*, 180–189. https://doi.org/10.1016/j.lithos.2019.02.004

References From the Supporting Information

Bloomer, S. H., & Fisher, R. L. (1987). Petrology and geochemistry of igneous rocks from the Tonga Trench: A non-accreting plate boundary. *The Journal of Geology*, *95*(4), 469–495. https://doi.org/10.2307/30081081

Dick, H. B., & Bullen, T. (1984). Chromian spinel as a petrogenetic indicator in abyssal and alpine-type peridotites and spatially associated lavas. *Contributions to Mineralogy and Petrology*, *86*(1), 54–76. https://doi.org/10.1007/BF00373711

Jaques, A. L., & Chappell, B. W. (1980). Petrology and trace element geochemistry of the Papuan Ultramafic Belt. *Contributions to Mineralogy and Petrology*, *75*(1), 55–70. https://doi.org/10.1007/BF00371889

Kamenetsky, V. S., Crawford, A. J., & Meffre, S. (2001). Factors controlling chemistry of magmatic spinel: An empirical study of associated olivine, Cr-spinel and melt inclusions from primitive rocks. *Journal of Petrology*, *42*(4), 655–671. https://doi.org/10.1093/petrology/42.4.655

Müntener, O., & Manatschal, G. (2006). High degrees of melt extraction recorded by spinel harzburgite of the Newfoundland margin: The role of inheritance and consequences for the evolution of the southern North Atlantic. *Earth and Planetary Science Letters*, *252*(3–4), 437–452. https://doi.org/10.1016/j.epsl.2006.10.009

Onyeagocha, A. C. (1978). Twin Sisters dunite: Petrology and mineral chemistry. *Geological Society of America Bulletin*, *89*(10), 1459–1474. https://doi.org/10.1130/0016-7606(1978)89<1459:tsdpam>2.0.co;2